Mechanical bending effects on hydrogen storage of Ni decorated (8, 0) boron nitride nanotube: DFT study

M. A. Tarek[1], H. O. Taha[1], M. A. Kamel[1] & A. M. El Mahdy[1,*]

[1] *Department of Physics, Faculty of Education, Ain Shams University, Roxy, 11341, Cairo, Egypt*
*Corresponding author. Email: a_m_elmahdy@hotmail.com; physics_depart@edu.asu.edu.eg

ABSTRACT

The influence of mechanical bending to tuning the hydrogen storage of Ni-functionalized of zigzag type of boron nitride nanotubes (BNNTs) has been investigated using density functional theory (DFT) with reference to the ultimate targets of the US Department of Energy (DOE). Single Ni atoms prefer to bind strongly at the axial bridge site of BN nanotube, and each Ni atom bound on BNNT may adsorb up to five, H_2 molecules, with average adsorption energies per hydrogen molecule of (-1.622,-0.527 eV) for the undeformed $B_{40}N_{40}$-φ = 0 , (-1.62 ,0 -0.308 eV) for the deformed $B_{40}N_{40}$-φ = 15, (-1.589, -0.310 eV) for the deformed $B_{40}N_{40}$-φ = 30, and (-1.368 - -0.323 eV) for the deformed $B_{40}N_{40}$-φ = 45 nanotubes respectively. with the H-H bonds between H_2 molecules significantly elongated. The curvature attributed to the bending angle has effect on average adsorption energies per H_2 molecule. With no metal clustering, the system gravimetric capacities are expected to be as large as 5.691 wt % for $5H_2$ Ni $B_{40}N_{40}$-φ = 0, 15, 30, 45. While the desorption activation barriers of the complexes nH_2 + Ni $B_{40}N_{40}$-φ = 0 (n = 1-4) are outside the (DOE) domain (-0.2 to -0.6 eV), the complexes nH_2 + Ni- $B_{40}N_{40}$-φ = 0 (n = 5) is inside this domain. For nH_2 + Ni- $B_{40}N_{40}$-φ = 15, 30, 45 with (n = 1-2) are outside the (DOE) domain, the complexes nH_2 + Ni- $B_{40}N_{40}$-φ = 15, 30, 45 with (n = 3-5) are inside this domain. The hydrogen storage of the irreversible $4H_2$+ Ni- $B_{40}N_{40}$-φ = 0, $2H_2$+ Ni- $B_{40}N_{40}$-φ = 15, 30, 45 and reversible $5H_2$+ Ni- $B_{40}N_{40}$-φ = 0, $3H_2$+ Ni- $B_{40}N_{40}$-φ = 15, 30, 45 interactions are characterized in terms of density of states, pairwise and non-pairwise additivity, infrared, Raman, electrophilicity and molecular electrostatic potentials. Our calculations expect that $5H_2$- Ni- $B_{40}N_{40}$-φ = 0, 15, 30, 45 complexes are promising hydrogen storage candidates.

Keywords: hydrogen storage; DFT; NBO; DOS; MEPs

*Corresponding author. Email: a_m_elmahdy@hotmail.com; physics_depart@edu.asu.edu.eg

1. Introduction

Carbon nanotubes (CNT) and boron nitride nanotubes (BNNT) have attracted much attention as candidates for a hydrogen storage media **[1,2]**. During the past decade, the carbon-based materials have been considered as promising media for hydrogen storage **[3, 4].** However, due to the very weak physical adsorption of H_2 for most materials including carbon-based materials, attention has been directed at non-carbon nanosystems composed of light elements such as B and N **[2]**. Boron nitride nanotubes (BNNTs) are inorganic analogues of carbon nanotubes (CNTs) **[5]**and possess physical properties suitable for a broad variety of applications **[6]**. Since theoretically predicted **[7]** and then successfully synthesized in 1995 **[8]**, BNNTs have attracted considerable attention due to the undisputed fact that in contrast to metallic or semi-conducting CNTs: BNNTs are wide-gap semiconductors with almost same band gaps of 5.5 eV, independent of the tube diameter, helicity, and the number of tube walls **[9]**, and they are chemically and thermally more stable **[7,10–12]**. Furthermore, the interaction of hydrogen molecules with material surfaces can be enhanced by heteropolar bonds at surfaces, a feature that is present in BNNTs but absent in CNTs. Given give these unique properties, as one of the most interesting non-carbon nanotubes **[13]**, BNNT has high potential practical application in hydrogen storage.

The hydrogen storage attracted much attention in recent years, especially. Ma et al. **[1]** measured the hydrogen storage ability of BN nanotubes and found that multiwall BN nanotubes can uptake 1.8–2.6 wt %

hydrogen under about 10 MPa at room temperature and 70% of adsorbed hydrogen is chemisorbed. In theoretical studies, Cheng et al.**[15]**obtained that capability of hydrogen storage in single-walled boron nitride nanotube arrays (SWBNNTA) can be increased with the increase of distance between BNNTs. Zhao and Ding **[16]** indicated that several gas molecules (H_2, O_2, and H_2O) dissociate and chemisorbs on BNNT edges, and the adsorption of these molecules induce a charge transfer. Yuan and Liew **[17]** reported that boron nitride impurities would cause a decrease in Young's moduli of SWCNTs. Moreover, the effect of these impurities in zigzag SWCNTs is more significant because of the linking characteristics of an increase in electrons. Mpourmpakis and Froudakis **[18]** discovered that BNNTs are preferable to CNTs for hydrogen storage because of the ionic character of BNNTs bonds, which can increase the binding energy of hydrogen. Also, some methods have been shown to improve the efficiency of storage. An increase in the diameter of BNNT can increase the efficiency of hydrogen storage **[19]**. Thus far, several hydrogen storage methods have been suggested. Further, Tang et al. **[20]** improved the concentration of hydrogen storage to 4.6 wt% by bending the BNNTs. BNNTs also have many great physical and chemical properties. Wu et al. **[21]** found that the radial deformation of BNNT significantly affects the H_2 adsorption energy on BNNT. They presented the relationship between the H_2 adsorption energy at different adsorption sites and the extent of radial deformation of BNNT. Ju et al.**[22]** have investigated the effect of uni-axial strain on the electronic properties of (8,0) zigzag and (5,5) armchair BNNT. They have found that the two different types of BNNTs show very similar mechanical properties and variations in HOMO–LUMO gaps at different strains.

Metal-functionalization has been found to be a beneficial scheme to improve or induce some unique properties of nanotubes**[23]**. Both experimental **[24-27]**and theoretical **[28,29]**studies were reported on the interaction of transition metal atoms with "perfect" BNNTs (BNNTs without intrinsic defects). The defective **[30 – 33]**, carbon-doped **[34,35]**, Si-doped **[32]**, Ti-doped **[36]**, Ni-doped **[37]**. The adsorption of Ni onto single-walled BNNTs with intrinsic defects has been studied using DFT calculations, and the results of that study were reported by Zhao and coworkers **[38]**. Zhang et al. **[39]** investigated Ni-functionalised single-walled boron nitride (BN) nanotubes and their applications for hydrogen storage by using DFT. They found that single Ni atoms prefer to bind strongly at the axial bridge site of BN nanotube (BNNT) and each Ni atom may adsorb up to three H_2 molecules. They also reported that the nature of the interaction between hydrogen and Ni-doped BNNT is due to the hybridisation of the metal d orbital with the hydrogen s orbital. W. Lei et al. **[40]** measured the hydrogen storage ability of oxygen doped boron nitride (BN) nanosheets with 2–6 atomic layers, synthesized by a facile sol-gel method and found that a storage capacity of 5.7 wt% under 5 MPa at room temperature and 89% of the stored hydrogen can be released when the hydrogen pressure is reduced to ambient conditions. Y. Liu et al. **[41]** investigated the hydrogen storage of Na-decorated single- and double-sided graphyne and their BN analogues. They found that the Na decorated double-sided graphyne and BN analogue the hydrogen storage capacities could reach to 5.98 and 5.84 wt%, with the average adsorption energies of 0.25 and 0.17 eV/H_2, respectively.

The main objective of the present work is to investigate the interactions between Ni and undeformed (φ = 0) and bending-deformed (φ = 15, 30 ,45) decorated single-walled zigzag (8,0) BNNT as well as between nH_2 and Ni– undeformed and bending-deformed (8,0) BNNT in terms of several structural and energetic properties such as bond lengths, natural bond orbital (NBO) charges, density of states (DOS), adsorption energies (Eads.) and energy gaps (highest occupied molecular orbital (HOMO)−lowest unoccupied molecular orbital (LUMO)). With reference to the ultimate targets of DOE for physisorption and gravimetric density, we have considered two types of reactions, namely reversible and irreversible, which were characterized in terms of NBO analysis of charges, densities of states (DOS), pairwise and non-pairwise additivities, infrared (IR), Raman (R), formation energy (ε), ionisation potential (I), electron affinity (A), chemical hardness (η), electronegativity (χ), electrophilicity (ω) and MEPs.

2. Computational methods

In this study, DFT methods are adopted to study the mechanical bending effects on hydrogen storage of Ni decorated single-walled zigzag BNNT. This method has been widely used in theoretical calculations of

nanotube systems, including structural and electronic properties. The DFT calculations were performed by using Becke's three-parameter exchange functional (B3) with Lee–Young–Parr (LYP) correlation functional [42-45]. The B3LYP hybrid functional has been chosen since it provides a rather accurate description of metal interactions. Hybrid functional such as B3LYP provides a fair indication of the relative energies, and in some cases, the resulting differences between the experimental values and the calculated ones can be considered a systematic error [46]. B3LYP correctly reproduces the thermochemistry of many compounds, including TM atoms [47– 49]. The advantages of employing DFT calculations for hydrogen storage materials research may be summarized as the accuracy of computed thermodynamic quantities, the efficiency relative to experiment, and thermodynamic predictions of new functionalized nanostructures [50]. We chose the finite cluster (8,0) zigzag BNNT with the length of 12 Å an including totally 40 boron, 40 nitrogen as the studied systems. Full geometry optimizations were carried out by using the larger B3LYP/6−31G(d,p) level of theory. The thresholds of geometry optimizations are: maximum force: 0.002500, root-mean-square (RMS) force: 0.001667; maximum displacements: 0.010000, RMS displacements: 0.006667. The convergence criteria of single point self consistent field (SCF) energy calculations are: RMS density matrix = 1.00E−07, MAX density matrix = 1.00E−05, and energy = 1.00E−05. The HOMO, the LUMO, and the energy gaps referred to as the energy difference between HOMO and LUMO ΔE (HOMO −LUMO) was also investigated at the same level of theory. Also, NBO analysis implemented in Gaussian 09 program [51] was applied to a series of intermolecular interactions under the above system to evaluate the NBO charges. All calculations were carried out by using the Gaussian 09 system [51]. The density of states (DOS) and Fermi levels were calculated by using Gauss Sum 2.2.5, which is a post-processing of Gaussian 09 code [52]. The optimal geometries were visualized by using the corresponding Gauss View 5.0 software.

3. Results and discussion

3.1. Interaction between Ni and BNNT-φ =0, 15, 30, 45

We constructed a zigzag BNNTs (8,0) with length 12 Å, B–N bond length 1.45 Å, consisting of 40 B and 40 N atoms and defined the bending angle in degrees (φ = 0) for the undeformed BNNT, and (φ = 15, 30, and 45) for the deformed BNNT. The frozen geometries of BNNT-φ = 0, BNNT-φ =15, 30, and 45 are shown in **Figure 1**.

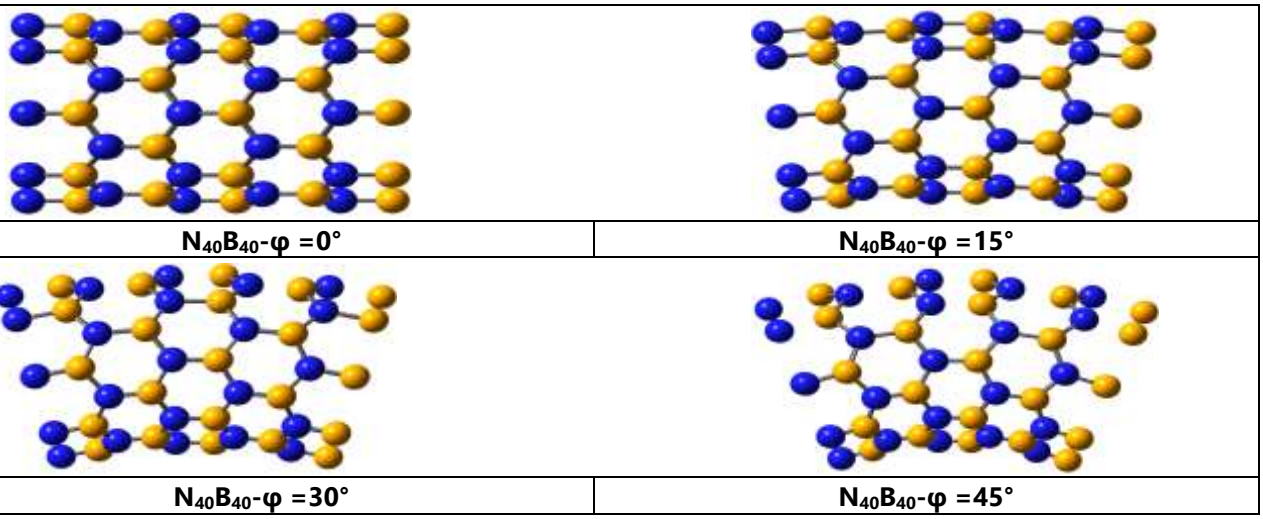

Figure 1. The geometries of $N_{40}B_{40}$-φ = 0, 15, 30, 45, BNNT = 0, 15, 30, 45 frozen cores. (For interpretation of the references to color in this figure legend, the reader is referred to the web version of this article.)

First, we analyzed the interaction between Ni atoms and (8, 0) BNNTs -φ = 0, 15, 30, and 45. Several various adsorption positions were selected for the Ni atom on the BNNTs as presented in **Figure 2**: (1) directly above

a boron atom (B), (2) above a nitrogen atom (N), (3) over an axial BN bond (A), (4) above a center of a hexagon (H), and over an zigzag BN bond (Z).

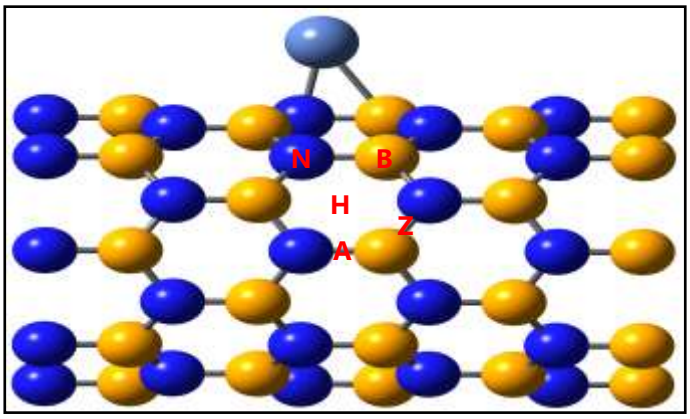

Figure 2. The optimized geometries of Ni- $N_{40}B_{40}$-φ = 0, BNNT = 0 frozen cores. In the figure and bellow figures, boron, nitrogen, and nickel are represented in gold, blue, and light blue color respectively. For interpretation of the references to color in this figure legend, the reader is referred to the web version of this article.)

It is found that the four adsorption configurations are stable. In order to evaluate the stability of the four configurations the binding energy is calculated, which is given by the following expression:

$$E_b = E[BNNT + Ni] - E[BNNT] - [Ni]$$

Where E[BNNT+Ni] is the total energy of the fully relaxed Ni-BNNT, and E[BNNT] and E[Ni] are the energies of the isolated systems. By definition, a negative value of E_b Corresponds to exothermic adsorption. For these sites in **Figure 3**, our calculations show that the adsorption of Ni is all exothermic.

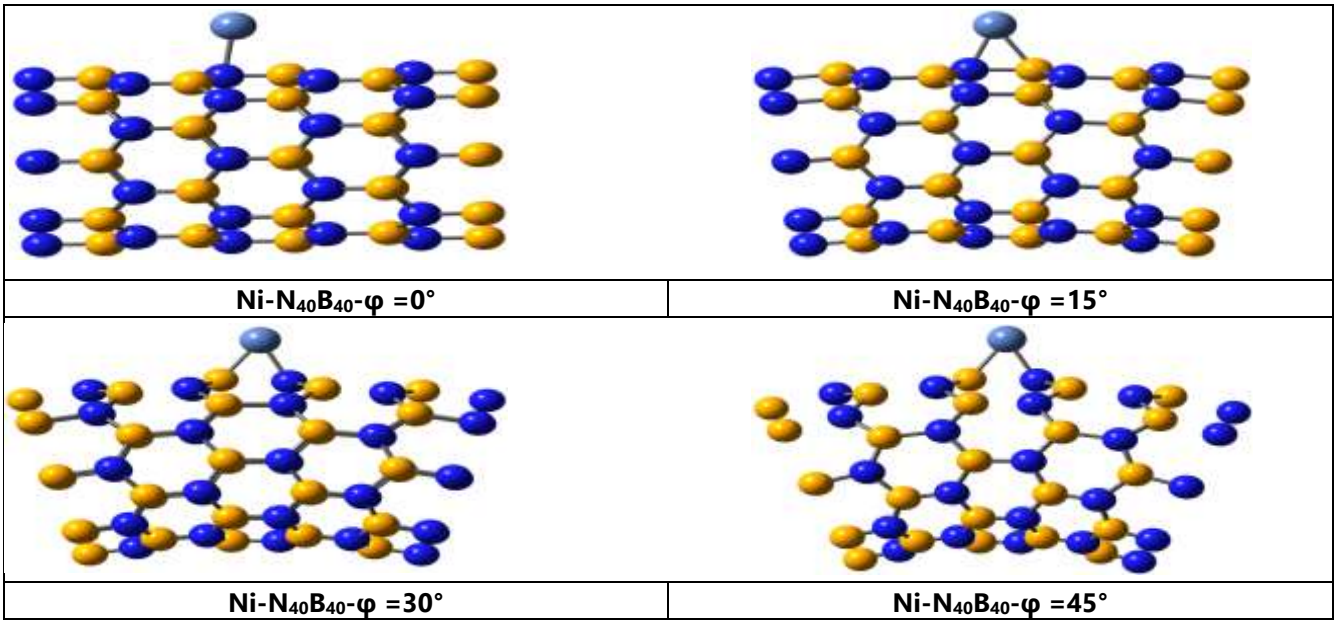

Figure 3. The optimized geometries of Ni- $N_{40}B_{40}$, -φ = 0, 15, 30, 45. (For interpretation of the references to color in this figure legend, the reader is referred to the web version of this article).

The binding energies for the most stable configurations BNNT-φ =0, 15, 30, 45 structures are summarized in **Table 1**. For the case of a Ni-BNNT- φ = 0 system, the adsorption energy at the A site is -4.81 eV with a bond length of B-Ni and N-Ni are 2.085 and 1.776 Å, respectively. This bond length is consistent with the results suggested by Zhao et al. **[28,38,53]** and the value predicted by Auwarter et al.**[54]**. For the Ni-BNNT- φ = 15 system, the adsorption energy at the N site is -6.041 eV with a bond length of B-Ni and N-Ni are 2.020 and 1.777 Å, respectively. The adsorption energy of the Ni-BNNT- φ = 30 at the H site is -4.693 eV with a bond

length of B-Ni and N-Ni are 1.907 and 1.765 Å, respectively. While for the Ni-BNNT- φ = 45 system, the adsorption energy at the Z site is -6.980 eV with bond lengths of Ni-B and Ni-N being 1.867 and 1.750 Å respectively. These optimized Nickel doped on BNNT- φ = 0,15,30,45 is taken as our model system, and the hydrogen molecules were added one by one to the doped Ni. The adsorption energy of Ni is significantly larger than the average adsorption energies of H_2 molecule (-0.61 and -0.21 eV) ensuring the stability of the BNNT- φ = 0,15,30,45 complexes in the event of H_2 molecule released, **Table 1**.

Table 1. Calculated binding energies (E_b, in eV), the Bond Lengths (in Å) of Ni-B and Ni-N Bonds, (total electronic energy, HOMO, LUMO, and energy gap (E_g) in eV), dipole moment (μ) in Debye and charge transferred (in a.u) from the Ni Atom to the BNNT at -φ = 0, 15, 30 and 45 complexes.

Structure	E_b	d(Ni-B)	d(Ni-N)	E (a.u.)	HOMO	LUMO	E_g	μ	Q_{Ni}
Ni-$B_{40}N_{40}$-φ = 0									
A-site	-4.810	2.085	1.776	-4694.15736469	-5.634	-5.318	0.316	6.431	0.496
Ni-$B_{40}N_{40}$-φ = 15									
N-site	-6.041	2.0198	1.777	-4693.68995546	-5.673	-5.357	0.316	84.788	0.345
Ni-$B_{40}N_{40}$-φ = 30									
H-site	-4.693	1.907	1.765	-4693.28803241	-5.741	-5.447	0.294	23.120	0.593
Ni-$B_{40}N_{40}$-φ = 45									
Z-site	-6.980	1.867	1.750	-4692.00397200	-5.680	-5.390	0.290	24.762	0.611

According to the Mulliken charge analysis of single Ni atom adsorbed on BNNT-φ = 0,15,30,45, Ni atom donates electrons to the neighboring boron and nitrogen atoms on the BNNT- φ = 0,15,30,45, and this charge transfer decreases form boron and nitrogen atoms far away from the metal atom. The d orbital's of Ni atom overlaps with the sp and sp3orbitals of the Ni-B and Ni-N bonds to form mixed (spd and sp3d)hybridization. This charge transfer behavior leads to Ni atom in cationic form and renders extensive heteropolar bonding between the Ni atom and the nearest boron and nitrogen atoms **(Figure 4)**.

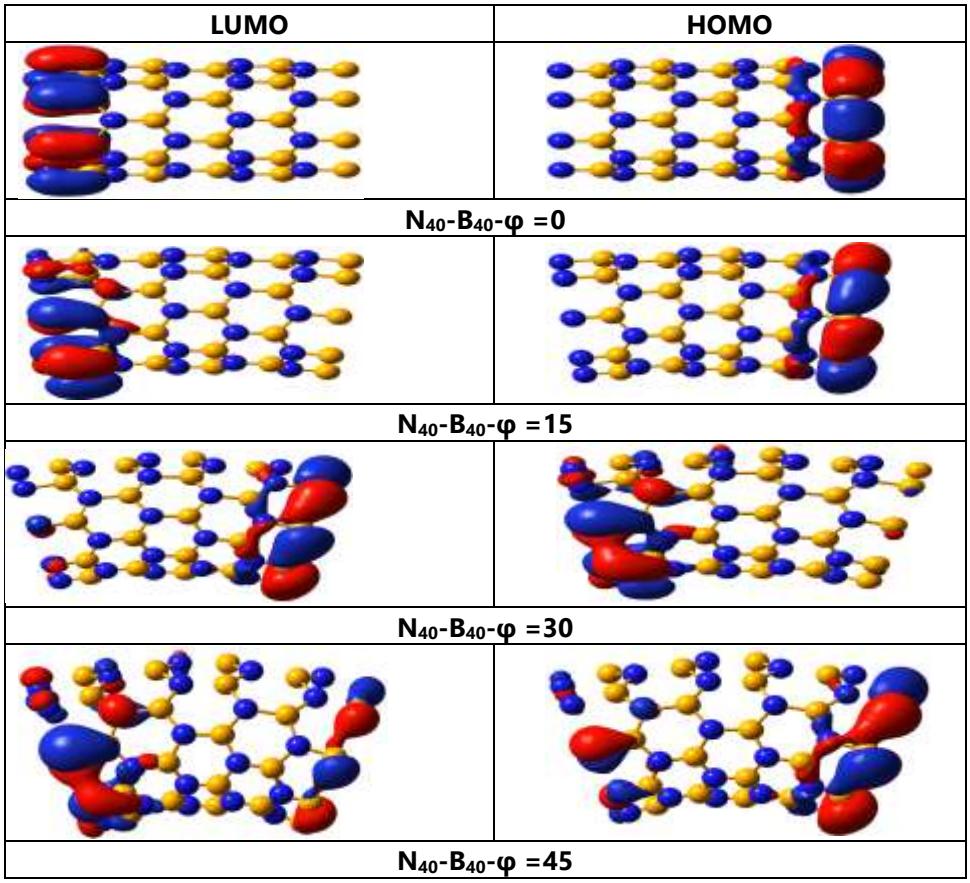

Figure 4. Frontier orbital isosurface plots of N_{40}-B_{40}-φ =0, 15, 30, 45 complexes.

As a consequence, extra dipole moments are formed, thus resulting in an increase in the H_2 molecule uptake.

It is well known that the frontier orbitals, the highest occupied molecular orbital (HOMO) and the lowest unoccupied molecular orbital (LUMO), play an important role in a chemical reaction to the reactant molecules, thus the frontier orbital analysis of the BNNT- φ = 0,15,30,45 is necessary. **In Table 2**, we summarize the HOMO and LUMO energy levels of the BNNT- φ = 0,15,30,45. It can be seen that HOMO levels of the BNNT- φ = 15, 30, 45 are all increased compared with that of pure BNNT- φ =0. As for LUMO levels of the BNNT- φ = 15, 30, 45 are all decreased compared with that of pure BNNT- φ =0.

Table 2. The obtained HOMO, LUMO, and energy gap (E_g).

Structure	HOMO	LUMO	E_g
$B_{40}N_{40}$-φ = 0	-5.616	-5.591	0.025
$B_{40}N_{40}$-φ = 15	-5.801	-5.534	0.267
$B_{40}N_{40}$-φ = 30	-5.848	-5.563	0.285
$B_{40}N_{40}$-φ = 45	-5.777	-5.511	0.266

Figure 4 shows the distributions of HOMO and LUMO for the BNNT- φ =0 and BNNT- φ = 15, 30, 45 studied in this paper. It can be seen that the frontier orbitals for undeformed BNNT-φ = 0 and deformed BNNT-φ =15 systems there is strong localization of the HOMOs on boron end of the BNNT and strong localization of the LUMOs on nitrogen end of the BNNT. While for deformed BNNT-φ = 30 there is strong localization of the HOMOs on nitrogen end of the BNNT and strong localization of the LUMOs on the Boron end of the BNNT. For the deformed BNNT-φ = 45 system, there is strong localization of the HOMOs and LUMOs on the two ends of the BNNT.

In Table 1, we summarize the HOMO and LUMO energy levels of the Ni-BNNT- φ = 0,15,30,45. It can be seen that HOMO levels of the Ni-BNNT- φ = 15, 30, 45 are all increased compared with that of pure BNNT- φ =0. While for LUMO levels of the Ni-BNNT- φ = 15, 30, 45 are all decreased compared with that of pure Ni-BNNT- φ =0. **Figure 5** shows the distributions of HOMO and LUMO for the Ni-BNNT- φ =0, 15, 30, 45 studied in this paper. It can be seen that the frontier orbitals for undeformed Ni-BNNT-φ = 0 system there is strong localization of the HOMOs on the two ends of the Ni-BNNT and strong delocalization of the Ni atom. While for LUMO levels there is strong localization on both Ni atom and BNNT- φ =0 tube. For deformed BNNT-φ = 15 system, there is strong localization of the HOMOs on both Ni atom and nitrogen end of the BNNT -φ = 15. While for LUMO levels there is strong localization on boron end of the BNNT -φ = 15 only. For deformed BNNT-φ = 30, 45 systems there is strong localization of the HOMOs, LUMO on Ni atom and the two ends of the BNNT-φ = 30, 45. The density of states analysis of BNNT and Ni atom-doped BNNT-φ = 0, 15, 30, 45 shows that electrons are transferred to BNNT-φ = 0,15,30,45 . BNNT-φ = 0,15,30,45 has 'p' orbitals alone, which are due to boron and, nitrogen atoms.

The reason for doping a transition element is that charges are transferred to BNNT-φ = 0,15,30,45 and this charge transfer makes the doping a positively charged ion. According to our NBO analysis, the charge on Ni is 0.496 (BNNT-φ = 0), 0.345(BNNT-φ = 15), 0.593 (BNNT-φ = 30), and 0.611 (BNNT-φ = 45) while on the nearest neighbour B around from 0.780 to 0.921, and for N from -1.170 to -1.213. This indicates that the Ni atom donates electrons to the neighboring N and B atom on BNNT-φ = 0,15,30,45. Where the d-orbitals of the Ni atom overlap with the (B sp and N sp3) orbitals of the Ni–Ni–B and Ni–N bonds, respectively.

This charges to transfer behavior leads to the Ni atom in cationic form and renders extensive heteropolar bonding with Ni atom and the nearest B and N atoms, resulting in an increase in the H_2 molecule uptake. Moreover, the BNNT-φ = 0,15,30,45 approaching the positively charged Ni cation leads to the loss of d-orbital degeneracy as the electrons of the BNNT-φ = 0,15,30,45 will be closer to some of the d-orbitals while farther

away from others. Thus, d-orbitals closer to the BNNT-φ = 0,15,30,45 has higher energy than those farther away.

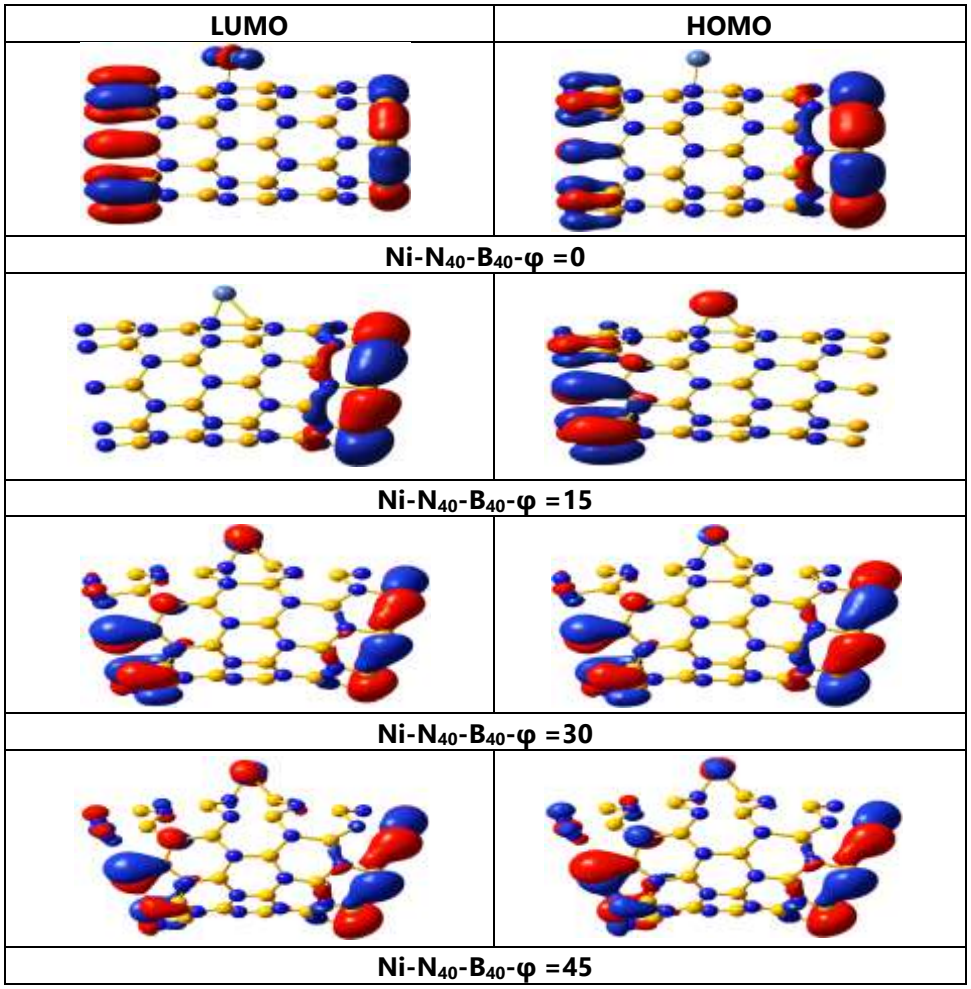

Figure 5. Frontier orbital isosurface plots of Ni-N_{40}-B_{40}-φ =0, 15, 30, 45 complexes.

3.2. Interactions between nH_2 and Ni - BNNT-φ = 0,15,30,45

The adsorption of hydrogen molecule on the stable configuration of Ni doped BNNT-φ = 0,15,30,45 system was studied (axial BN bond (A) for BNNT-φ = 0, (N) site for BNNT-φ = 15, (H) site for BNNT-φ = 30 and (Z) site for BNNT-φ = 45). The optimized nH_2 Ni BNNT-φ = 0,15,30,45 complexes are shown in **Figures (6)**.

The average adsorption energy of H_2 over the Ni-BNNT is defined as

$$\Delta E_{ads}(H_2) = [E(nH_2 - Ni - BNNT) - E(Ni - BNNT) - nE(H_2)]/n \quad (1)$$

where $E(nH_2 - Ni - BNNT)$ is the total energy of the fully relaxed $nH_2 - Ni$ fragment deposited on frozen BNNT, $E(H_2)$ is the energy of an isolated relaxed hydrogen molecules, $E(Ni - BNNT)$ Is the total energy of the fully relaxed Ni atom deposited on frozen BNNT and (n) is the number of hydrogen molecules. By definition, negative adsorption energy corresponds to an exothermic adsorption.

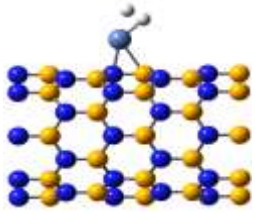	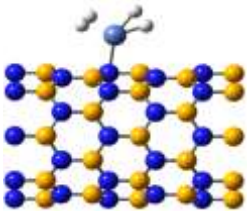	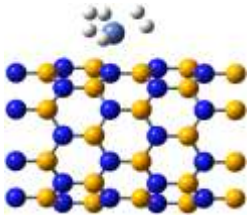	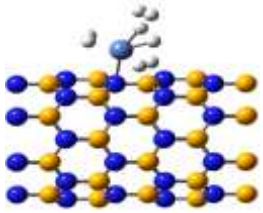
$1H_2$-Ni-$N_{40}B_{40}$-φ =0	$2H_2$-Ni-$N_{40}B_{40}$-φ =0	$3H_2$-Ni-$N_{40}B_{40}$-φ =0	$4H_2$-Ni-$N_{40}B_{40}$-φ =0
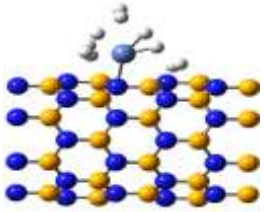			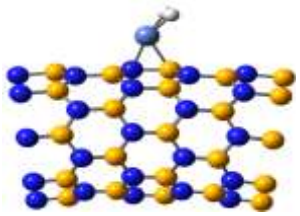
$5H_2$-Ni-$N_{40}B_{40}$-φ =0			$1H_2$-Ni-$N_{40}B_{40}$-φ =15
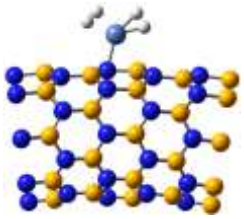	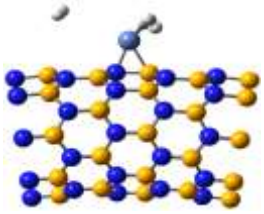	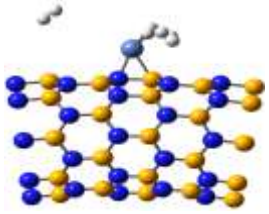	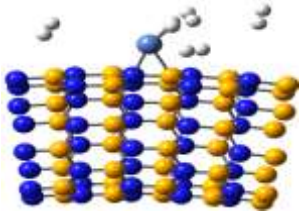
$2H_2$-Ni-$N_{40}B_{40}$-φ =15	$3H_2$-Ni-$N_{40}B_{40}$-φ =15	$4H_2$-Ni-$N_{40}B_{40}$-φ =15	$5H_2$-Ni-$N_{40}B_{40}$-φ =15
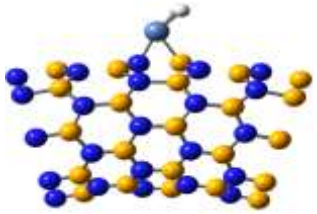	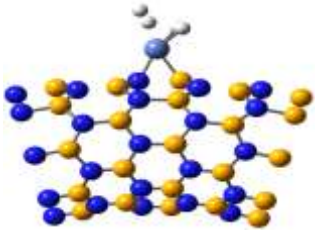	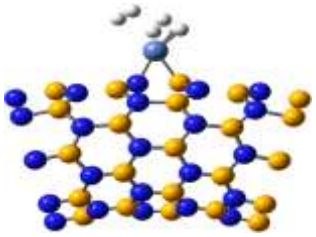	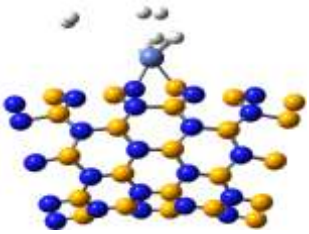
$1H_2$-Ni-$N_{40}B_{40}$-φ =30	$2H_2$-Ni-$N_{40}B_{40}$-φ =30	$3H_2$-Ni-$N_{40}B_{40}$-φ =30	$4H_2$-Ni-$N_{40}B_{40}$-φ =30
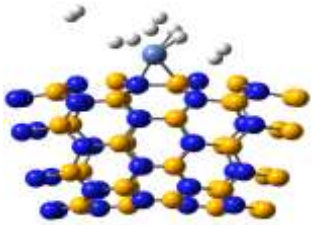			
$5H_2$-Ni-$N_{40}B_{40}$-φ =30			$1H_2$-Ni-$N_{40}B_{40}$-φ =45
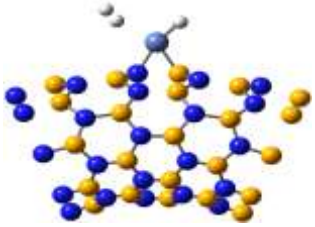	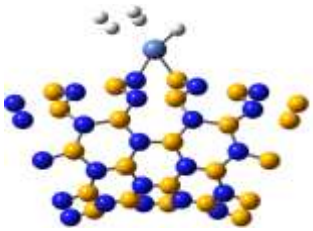	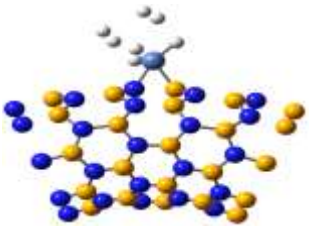	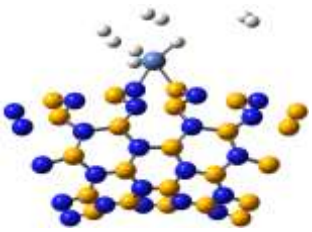
$2H_2$-Ni-$N_{40}B_{40}$-φ =45	$3H_2$-Ni-$N_{40}B_{40}$-φ =45	$4H_2$-Ni-$N_{40}B_{40}$-φ =45	$5H_2$-Ni-$N_{40}B_{40}$-φ =45

Figure 6. The optimized geometries of nH_2-Ni-$N_{40}B_{40}$-φ =0,15, 30, 45 (n = 1–5) complexes.

3.2.1. Undeformed nH_2-Ni- BNNT-φ = 0

As shown in **Table 3**, the first, second , third and fourth H_2 molecule are adsorbed over an axial BN bond (A site) with adsorption energies of -1.622, -1.296 , -1.043 and -0.663 eV respectively, are larger than DOE requirement (-0.20 to -0.60 eV) and H_2 bond length in the four complexes (0.875Å, (0.826, 0.917 Å) , (0.836, 0.839, 0.865 Å), (0.742, 0.743, 0.810, 0.941 Å) increased relative to the experimental bond length of 0.74 Å **[55]**. The corresponding distance between Ni to the nearest boron is (2.125, 2.248, 2.438 and 2.257 Å) and to the nearest nitrogen are (1.839, 1.939, 1.950 and 2.059 Å) respectively. Compared with the Ni- BNNT-φ = 0 in the absence of H_2 molecule, the adsorption of H_2 molecule weakens the interaction between Ni- BNNT-φ = 0. The sp3d hybridization of the Ni–B and Ni–N bonds, respectively seems to have repulsive effects on the adsorbed H_2 leading to the elongation of the H–H distance between 0.810 and 0.941 Å. Furthermore, Ni-doped BNNT-φ = 0 is not suitable for first, second, third, and fourth hydrogen molecules adsorption. When more H_2 molecule is adsorbed on Ni-BNNT-φ = 0, **Table 3**, the adsorption energy for H_2 molecules decreases to -0.527 eV upon adsorption of the fifth H_2.

The Ni atom may, therefore, bind up to five H_2 molecules. While the average adsorption energies are decreasing functions of the H_2 coordination number, the charges of Ni atoms display an oscillatory behavior.

3.2.2. Deformed nH_2-Ni- BNNT-φ = 15, 30, 45

a) nH_2-Ni- BNNT-φ = 15

For the deformed nH_2-Ni- BNNT-φ = 15, **Table 4**, the first, and the second H_2 molecule are adsorbed on the stable configuration of Ni-doped BNNT-φ = 15 (N site)
with adsorption energies of -1.620, and -1.222 eV respectively, is larger than DOE requirement (-0.20 to -0.60 eV), and H_2 bond length in the two complexes (0.872, and (0.903,0.834) Å) increased relative to the original one (0.74 Å). The corresponding distance between Ni to the nearest boron and nitrogen is (2.198, 1.995), and (1.907, 1.844) Å respectively. Compared with the Ni- BNNT-φ = 15 in the absence of H_2 molecule, the adsorption of H_2 molecule weakens the interaction between Ni- BNNT-φ = 15. When more than one H_2 molecule is adsorbed on Ni- BNNT-φ = 15, the average adsorption energies for each H_2 molecule decrease in -0.542, -0.409 and -0.308 eV upon adsorption of the third, fourth and fifth H_2 molecule respectively. The Ni atom may, therefore, bind up to five H_2 molecules. The average adsorption energies per H_2 molecule (-0.542, -0.409 and -0.308 eV) meets the ultimate targets of DOE for physisorption (−0.20 to −0.60 eV) and nominate Ni- BNNT-φ = 15 as potential hydrogen storage materials.

b) nH_2-Ni- BNNT-φ = 30

For the deformed nH_2-Ni- BNNT-φ = 30, **Table 5**, the first, and the second H_2 molecule are adsorbed on the stable configuration of Ni-doped BNNT-φ = 30 (H site)
with adsorption energies of -1.589, and -0.800 eV respectively, is larger than DOE requirement (-0.20 to -0.60 eV), and H_2 bond length in the two complexes (0.864, and 0.861 Å) increased relative to the original one (0.74 Å). The corresponding distance between Ni to the nearest boron and nitrogen is (1.908, 1.837), and (1.906, 1.838) Å respectively. Compared with the Ni- BNNT-φ = 30 in the absence of H_2 molecule, the adsorption of H_2 molecule weakens the interaction between Ni- BNNT-φ = 30. When more than one H_2 molecule is adsorbed on Ni- BNNT-φ = 30, the average adsorption energies for each H_2 molecule decrease in -0.530, -0.401 and -0.249 eV upon adsorption of the third, fourth and fifth H_2 molecule respectively. The Ni atom may, therefore, bind up to five H_2 molecules. The average adsorption energies per H_2 molecule (-0.530, -0.401 and -0.249 eV) meets the ultimate targets of DOE for physisorption (−0.20 to −0.60 eV) and nominate Ni- BNNT-φ = 30 as potential hydrogen storage materials.

Table 3. Structural and energetic parameters of the optimized nH_2 Ni-$N_{40}B_{40}$-φ = 0 systems (n=1-5). All distances (d) are given in Å , energies ($E_{ads.}$, HOMO, LUMO, and E.G) in eV, natural bond order charges (Q) in au, and dipole moment (μ) in Debye. The average adsorption energy $E_{ads.}$ per hydrogen molecule in eV.

Systems	$\Delta E_{ads.}$	d(Ni-B)	d(Ni-N)	d(Ni-H)	d(H-H)	Q_{Ni}	Q_B	Q_N	Q_{H-H}	HOMO	LUMO	E.G	μ
Ni-$N_{40}B_{40}$-φ = 0	-4.810	2.085	1.776	1.588,1.569	0.840	0.251	0.338	-0.57	----	-5.634	-5.318	0.316	18.471
1H_2 Ni-$N_{40}B_{40}$-φ = 0	-1.622	2.125	1.839	1.492 , 1.540	0.875	0.474	0.951	-1.196	-0.0241 ,-.0563	-5.709	-5.436	0.273	18.165
2H_2 Ni-$N_{40}B_{40}$-φ = 0	-1.296	2.248	1.939	1.525 , 1.518 1.603 , 1.591	0.917 0.826	0.321	0.969	-1.177	- 0.0007, 0.0203 - 0.0199,- 0.0168	-5.725	-5.450	0.275	17.844
3H_2 Ni-$N_{40}B_{40}$-φ = 0	-1.043	2.438	2.059	1.583 , 1.562 1.608 , 1.608 1.613 , 1.613	0.865 0.839 0.836	-0.010	1.051	-1.168	0.0419, 0.0277 0.0419 , 0.0277 0.0148, 0.0459	-5.728	-5.457	0.271	18.613
4H_2 Ni-$N_{40}B_{40}$-φ = 0	-0.663	2.257	1.950	1.514 , 1.503 1.621 , 1.618 4.070 , 3.729 4.057 , 3.718	0.941 0.810 0.743 0.742	0.336	0.968	-1.182	- 0.0343,- 0.0298 0.0150, 0.0134 0.0081,- 0.0063 0.0076,- 0.0059	-5.726	-5.453	0.273	18.283
5H_2 Ni-$N_{40}B_{40}$-φ = 0	-0.527	2.250	1.941	1.524 , 1.517 1.604 , 1.590 4.132 , 3.412 4.417 , 3.675 4.553 , 3.852	0.920 0.827 0.744 0.743 0.743	0.334	0.968	-1.180	-0.0245 , -0.0197 0.0166 , -0.0176 0.0109 , -0.0119 -0.0099 , 0.0094 -0.0045 , 0.0166	-5.721	-5.451	0.270	18.552

Table 4. **Structural and energetic parameters of the optimized nH_2 Ni-$N_{40}B_{40}$-φ = 15 systems (n=1-5). All distances (d) are given in Å, energies ($E_{ads.}$, HOMO, LUMO and e.g.) in eV, natural bond order charges (Q) in au, and dipole moment (μ) in Debye. The average adsorption energy $E_{ads.}$ per hydrogen molecule in eV.**

Systems	$\Delta E_{ads.}$	d(Ni-B)	d(Ni-N)	d(Ni-H)	d(H-H)	Q_{Ni}	Q_B	Q_N	Q_{H-H}	HOMO	LUMO	E.G	μ
Ni-$N_{40}B_{40}$-φ = 15	-6.041	2.098	1.777	-	-	0.279	0.372	-0.675	-	-5.673	-5.357	0.316	20.213
1H_2 Ni-$N_{40}B_{40}$-φ = 15	-1.620	1.995	1.844	1.516 , 1.513	0.872	0.481	0.911	-1.238	-0.0358 , -0.0353	-5.777	-5.499	0.278	21.034
2H_2 Ni-$N_{40}B_{40}$-φ = 15	-1.222	2.198	1.907	1.534 , 1.518 1.605 , 1.590	0.834 0.903	0.324	0.956	-1.216	-0.0077 , 0.0079 -0.0022 , 0.0144	-5.786	-5.510	0.276	20.579
3H_2 Ni-$N_{40}B_{40}$-φ = 15	-0.542	1.992	1.845	1.518 , 1.521 3.678 , 3.578 3.834 , 4.210	0.742 0.744 0.871	0.485	0.911	-1.242	0.0058 , -0.0001 -0.0075 , 0.0085 -0.0402 , -0.0411	-5.771	-5.494	0.277	20.549
4H_2 Ni-$N_{40}B_{40}$-φ = 15	-0.409	1.990	1.843	1.518 , 1.521 3.871 , 4.481 4.194 , 4.465 4.653 , 4.815	0.744 0.744 0.744 0.867	0.488	0.910	-1.241	-0.0381 , -0.0384 -0.0078 , 0.0093 -0.0091 , 0.0082 -0.0042 , 0.0047	-5.776	-5.495	0.281	20.109
5H_2 Ni-$N_{40}B_{40}$-φ = 15	-0.308	1.979	1.833	1.520 , 1.516 4.137 , 4.677 4.191 , 4.350 4.803 ,4.942 4.988 , 4.614	0.732 0.742 0.757 0.751 0.856	0.483	0.908	-1.239	-0.0376 , -0.0315 0.0181 , -0.0065 -0.0084 , 0.0081 -0.0043 , 0.0047 0.0073 , -0.0092	-5.775	-5.498	0.276	21.161

Table 5. Structural and energetic parameters of the optimized nH_2 Ni-$N_{40}B_{40}$-φ = 30 systems(n=1-5). All distances (d) are given in Å, energies ($E_{ads.}$, HOMO, LUMO and, e.g.) in eV, natural bond order charges (Q) in au, and dipole moment (μ) in Debye. The average adsorption energy $E_{ads.}$ Per hydrogen molecule in eV.

Systems	$\Delta E_{ads.}$	d(Ni-B)	d(Ni-N)	d(Ni-H)	d(H-H)	Q_{Ni}	Q_B	Q_N	Q_{H-H}	HOMO	LUMO	E.G	μ
Ni-$N_{40}B_{40}$-φ = 30	-4.693	1.907	1.765	-	-	0.310	0.360	-0.715	-	-5.741	-5.447	0.294	23.855
$1H_2$ Ni-$N_{40}B_{40}$-φ = 30	-1.589	1.908	1.837	1.525 , 1.522	0.864	0.507	0.871	-1.247	-0.0261 , -0.0230	-5.804	-5.520	0.283	23.096
$2H_2$ Ni-$N_{40}B_{40}$-φ = 30	-0.800	1.906	1.838	1.523 , 1.526 4.197 , 4.294	0.743 0.861	0.509	0.871	-1.247	-0.0014 , 0.0024 -0.0236 , -0.0266	-5.801	-5.519	0.282	23.329
$3H_2$ Ni-$N_{40}B_{40}$-φ = 30	-0.530	1.907	1.840	1.525 ,1.526 4.006 , 4.170 4.849 , 5.094	0.743 0.743 0.861	0.509	0.871	-1.248	-0.0255 , -0.0264 -0.0012 , 0.0064 -0.0049 , 0.0014	-5.799	-5.516	0.283	23.362
$4H_2$ Ni-$N_{40}B_{40}$-φ = 30	-0.401	1.905	1.840	1.522 , 1.525 4.064 , 4.037 4.561 , 4.383 4.975 , 5.238	0.743 0.743 0.743 0.861	0.511	0.871	-1.249	-0.0253 , -0.0277 -0.0011 , 0.0048 -0.0041 , 0.0012 -0.0009 , 0.0029	-5.797	-5.515	0.282	22.713
$5H_2$ Ni-$N_{40}B_{40}$-φ = 30	-0.249	1.909	1.837	1.521 , 1.527 3.783 ,4.344 3.978 , 4.038 4.105 , 4.300 4.437 , 4.857	0.743 0.744 0.745 0.746 0.862	0.517	0.869	-1.251	-0.0277 , -0.0302 -0.0038 , 0.0055 -0.0040 , 0.0033 -0.0024 , 0.0047 -0.0054 , 0.0046	-5.798	-5.498	0.300	46.066

Table 6. **Structural and energetic parameters of the optimized nH_2 Ni-$N_{40}B_{40}$-φ = 45 systems (n=1-5). All distances (d) are given in Å, energies ($E_{ads.}$, HOMO, LUMO, and e.g.) in eV, natural bond order charges (Q) in au, and dipole moment (μ) in Debye. The average adsorption energy $E_{ads.}$ Per hydrogen molecule in eV.**

Systems	$\Delta E_{ads.}$	d(Ni-B)	d(Ni-N)	d(Ni-H)	d(H-H)	Q_{Ni}	Q_B	Q_N	Q_{H-H}	HOMO	LUMO	E.G	μ
Ni-$N_{40}B_{40}$-φ = 45	-6.980	1.867	1.750	-	-	0.296	0.398	-0.715	-	-5.680	-5.390	0.290	25.531
$1H_2$ Ni-$N_{40}B_{40}$-φ = 45	-1.368	1.919	1.784	1.524 , 1.570	0.841	0.501	0.843	-1.244	0.0136 , -0.0287	-5.741	-5.454	0.286	23.702
$2H_2$ Ni-$N_{40}B_{40}$-φ = 45	-0.800	1.904	1.827	1.534 ,1.535 2.090 , 2.808	0.750 0.852	0.483	0.849	-1.256	-0.0122, -0.0132 -0.0852 , 0.0809	-5.737	-5.454	0.283	24.087
$3H_2$ Ni-$N_{40}B_{40}$-φ = 45	-0.528	1.902	1.827	1.533 , 1.533 2.194 , 2.918 2.869 , 3.611	0.745 0.748 0.851	0.485	0.849	-1.259	-0.0179 ,-0.0140 -0.0771 ,0.0747 0.0267 , -0.0312	-5.738	-5.455	0.283	24.635
$4H_2$ Ni-$N_{40}B_{40}$-φ = 45	-0.404	1.905	1.830	1.534 , 1.535 2.091 , 2.809 4.058 , 4.430 4.067 , 4.458	0.743 0.743 0.749 0.853	0.487	0.848	-1.258	-0.0152 , -0.0142 -0.0849 , 0.0815 -0.0024 , 0.0016 0.0075 , -0.0064	-5.738	-5.455	0.283	24.592
$5H_2$ Ni-$N_{40}B_{40}$-φ = 45	-0.323	1.903	1.829	1.535 , 1.535 2.088 , 2.794 4.094 , 4.487 4.045 , 4.445 4.966 , 4.981	0.743 0.743 0.744 0.750 0.851	0.486	0.847	-1.258	-0.0152 , -0.0127 -0.0836 , 0.0811 -0.0021 , 0.0011 0.0081 , -0.0070 0.0019 , -0.0016	-5.737	-5.452	0.284	24.341

c) nH₂-Ni- BNNT-φ = 45

For the deformed nH2-Ni- BNNT-φ = 45, **Table 6**, the first, and the second H_2 molecule are adsorbed on the stable configuration of Ni-doped BNNT-φ = 45 (Z site)
With adsorption energies of -1.368, and -0.800 eV respectively, is larger than DOE requirement (-0.20 to -0.60 eV), and H_2 bond length in the two complexes (0.852, and 0.841 Å) increased relative to the original one (0.74 Å). The corresponding distance between Ni to the nearest boron and nitrogen is (1.904, 1.902), and (1.827, 1.822) Å respectively. Compared with the Ni- BNNT-φ = 45 in the absence of H_2 molecule, the adsorption of H_2 molecule weakens the interaction between Ni- BNNT-φ = 45. When more than one H_2 molecule is adsorbed on Ni- BNNT-φ = 45, the average adsorption energies for each H_2 molecule decrease in -0.528, -0.404 and -0.323 eV upon adsorption of the third, fourth and fifth H_2 molecule respectively. The Ni atom may, therefore, bind up to five H_2 molecules. The average adsorption energies per H_2 molecule (-0.528, -0.404 and -0.323 eV) meets the ultimate targets of DOE for physisorption (−0.20 to −0.60 eV) and nominate Ni- BNNT-φ = 30 as potential hydrogen storage materials.
Our calculation results show that the average adsorption energies per H_2 of the undeformed $5H_2$-Ni-BNNT-φ= 0 (-0.527 eV) are greater than the deformed $5H_2$-Ni-BNNT-φ =15, 30 and 45(-0.308, -0.249, -0.323 eV) respectively. The adsorption energies of the deformed $5H_2$-Ni-BNNT-φ = 45 are greater than those with the deformed $5H_2$-Ni-BNNT-φ =15, and 30). This implies that the adsorption property of the deformed $5H_2$-Ni-BNNT is either correlated with the values of the bending angle, which increases to the direction φ =0 <φ =45 < φ =15 <φ =30. Also, our calculation results show that the curvature effects are affected on the adsorption energies, and these effects are cannot negligible. The adsorption energies of Ni atom deposited on BNNT-φ = 0 and BNNT-φ = 15, 30, 45 (-4.810, -6.041, -4.693, and -6.980 eV) are significantly greater than the average adsorption energies per H_2 molecule (-0.527, -0.308, -0.249, -0.323 eV) ensuring the stability of the Ni-BNNT complex in the event of H_2 molecule release. The average adsorption energies per H_2 molecule meets the ultimate targets of DOE for physisorption (−0.20 to −0.60 eV). The mechanical bending effects of the BNNT have significantly affected the distances between Ni and the nearest neighbour B and N atoms of the frozen BNNT.
The positive charges on Ni atoms are (0.334, 0.483, 0.517, 0.486), while the negative charges on the nearest neighbour N are (-1.180,-1.239,-1.251,-1.258) and the positive charges on the nearest neighbor B (0.968, 0.908, 0.869 and 0.847) for (φ = 0, 15, 30, 45) respectively obtained from natural bond orbital (NBO) analysis ensures charge transfer of Ni to the BNNT, **Tables 4-6**. This indicates that the Ni atom donates electrons to the neighbor N and B atoms on BNNT, Where the highest d orbital energy levels are given between round brackets, **Table 7**. These d orbitals are therefore the most probable d orbitals involved in the mixed (spd) and (sp3d) hybridization between B sp, N sp3, and Ni d. This charge transfer behavior leads to Ni atom in cationic form and renders extensive heteropolar bonding between Ni atom and the nearest neighbour N and B atoms, resulting in an increase in the H_2 molecule uptake. NBO analysis also suggested that interaction of H_2 over Ni- -φ =0, 15, 30, 45 are almost free of charge transfer interaction.

Table 7. Ni d-orbital energy (au) in the complexes nH_2-Ni- $N_{40}B_{40}$ -φ = 0, 15, 30 and 45, (n=1-5).

Systems Pure φ = 0	$1H_2$-Ni- $N_{40}B_{40}$	$2H_2$-Ni- $N_{40}B_{40}$	$3H_2$-Ni- $N_{40}B_{40}$	$4H_2$-Ni- $N_{40}B_{40}$	$5H_2$-Ni- $N_{40}B_{40}$
d_{xy}	1.669	1.684	1.767	1.709	1.692
d_{xz}	(1.950)	1.895	1.829	1.825	1.891
d_{yz}	1.936	(1.911)	(1.914)	(1.920)	(1.904)
$d_{x^2-y^2}$	1.610	1.555	1.695	1.577	1.555
d_{z^2}	1.694	1.786	1.569	1.799	1.790
φ = 15					
d_{xy}	1.541	1.607	1.546	1.544	1.518
d_{xz}	(1.871)	1.914	1.856	1.858	1.847
d_{yz}	1.795	(1.914)	1.787	1.788	1.802

$d_{x^2-y^2}$	1.858	1.585	(1.870)	(1.866)	(1.893)
d_{z^2}	1.788	1.789	1.796	1.797	1.797
φ = 30					
d_{xy}	1.441	1.444	1.445	1.455	1.451
d_{xz}	1.856	1.859	1.861	1.863	1.867
d_{yz}	1.803	1.805	1.804	1.800	1.803
$d_{x^2-y^2}$	(1.911)	(1.914)	(1.905)	(1.897)	(1.899)
d_{z^2}	1.826	1.816	1.823	1.823	1.815
φ = 45					
d_{xy}	1.443	1.404	1.406	1.405	1.392
d_{xz}	(1.958)	1.848	1.846	1.849	1.839
d_{yz}	1.932	1.815	1.815	1.815	1.826
$d_{x^2-y^2}$	1.717	(1.928)	(1.927)	(1.926)	(1.938)
d_{z^2}	1.770	1.838	1.838	1.839	1.838

To improve the hydrogen storage capacity, metal clustering should be avoided. We have examined systems containing two Ni atoms per cell. The metal atoms are placed using the energetically most favorable location obtained from the optimization of a single atom adsorbed on BNNT, namely, the A site (over an axial BN bond) for BNNT-φ = 0. Full geometry optimizations at the B3LYP/6-31g (d,p) level of theory were performed for the complexes nH_2Ni_2 BNNT-φ =0 (n = 2,4, 6, 8,10).

The gravimetric hydrogen storage capacity defined as the amount of hydrogen stored per unit mass of material was calculated from the relation

$$\mathrm{Wt\%} = \left[\frac{\mathrm{nlM_{H_2}}}{\mathrm{nlM_{H_2} + lM_{Ni} + m(M_B + M_N)}}\right] \times 100 \qquad (2)$$

where n is the number of H_2 molecules adsorbed on each Ni atom, l is the number of Ni atoms and m is the number of boron or nitrogen atoms, and M is the atomic or molecular weight. The average adsorption energies of 2, 4, 6, 8, and 10 hydrogen molecules, geometric parameters, and the expected hydrogen storage capacities are collected in **Table 8**. For the complexes, nH_2 + (Ni_2 –BNNT) (n = 10), the hydrogen storage capacities are expected to be as large as 5.691 wt %. However, it must be mentioned that metal atoms may tend to aggregate into clusters when their concentration is large. Hence, the hydrogen storage capacities achieved in these ideal circumstances might be reduced once metal clustering occurs.

Table 8. Average adsorption energies per H_2 ($E_{ads.}$), Ni - Ni distance d(Ni - Ni) and the expected hydrogen storage capacity $(wt\ \%)$ of the complex nH_2- Ni_2-$N_{40}B_{40}$ (n=2,4,6,8,10), Energies are given in eV and lengths in Å.

Systems	$\Delta E_{ads.}$	d(Ni–Ni)	$wt\ \%$
$2H_2$- Ni_2-$N_{40}B_{40}$	-1.636	4.67374	1.193
$4H_2$- Ni_2-$N_{40}B_{40}$	-0.859	4.67966	2.357
$6H_2$- Ni_2-$N_{40}B_{40}$	-0.574	4.68604	3.494
$8H_2$- Ni_2-$N_{40}B_{40}$	-0.433	4.67904	4.605
$10H_2$- Ni_2-$N_{40}B_{40}$	-0.349	4.67973	5.691

3.3. The characterization of nH_2 interactions with BNNT-φ =0, 15, 30, 45

Two types of interactions between nH_2 and BNNT-φ =0,15,30,45 could be identified from **Tables (3-6)** :(i) irreversible interactions between nH_2 (n=4) and Ni-BNNT-φ =0 , nH_2 (n=2) and Ni-BNNT-φ =15,30,45 (ii) reversible interactions between nH_2 (n=5) and Ni-BNNT-φ =0 , nH_2 (n=3-5) and Ni-BNNT-φ =15,30,45. Irreversible interactions are outside the desirable energy window (-0.2 to - 0.6 eV) recommended by DOE for practical applications, while the reversible interactions are inside. To characterize the nature of the two types of interactions, we considered the following theoretical descriptors (1) density of states DOS and frontier

orbitals, (2) pairwise and nonpairwise additivity (3) infrared and proton magnetic resonance spectra (4) electrophilicity (5) Molecular Electrostatic Potentials MEPs for the interactions of $4H_2$ and $5H_2$ with Ni-BNNT-φ =0, and for the interactions of $2H_2$ and $3H_2$ with Ni-BNNT-φ =15, 30, 45.

3.3.1. DOS and frontier molecular orbitals (FMOs)

The energy difference between the highest occupied molecular orbital (HOMO) and the lowest unoccupied molecular orbital (LUMO) can be considered a good indicator of changes in electronic properties and chemical reactivity **[56]**. In general, band gaps are governed by molecular structure, and the theoretical size of the bandgap defines the transition (excitation) energy from the ground state to the first dipole-allowed excited state **[57]**. However, the crudest estimates albeit the one most widely used due to its low computational costs based on the energy difference between the highest occupied molecular orbital (HOMO) and the lowest unoccupied molecular orbital (LUMO).

An understanding of the distribution of frontier orbitals around BNNTs would be valuable as it could be used to guide the design and characterization of new functionalized BNNTs for hydrogen storage. Frontier orbital isosurface plots of the present complexes are presented in **Figures (7-8)**. For undeformed and deformed BNNT-φ =0,15,30,45 system, there is strong localization of the HOMOs and LUMOs on the two ends of the BNNT, while there is strong delocalization of the HOMOs and LUMOs on Ni and H_2 fragments. This implies a significant flow of electronic charge across the interface between the Ni fragment and the BNNTs BNNT-φ = 0, 15, 30, 45.

The total DOS of a system describes the number of states per interval of energy at each energy level that is available to be occupied by electrons. A high DOS at a specific energy level means that there are many states available for occupation at that level. The density of states (DOS) is presented in **Figures (9, 10)**. A significant reduction in the energy gap is observed when the NiH_2 fragment is adsorbed onto the BNNTs. This reduction would be explained by a higher density of states near the Fermi level, which arises from the overlap between the 3d electrons of Ni and the nearest of B sp, N sp3 of the BNNTs **Figures (9, 10)**.

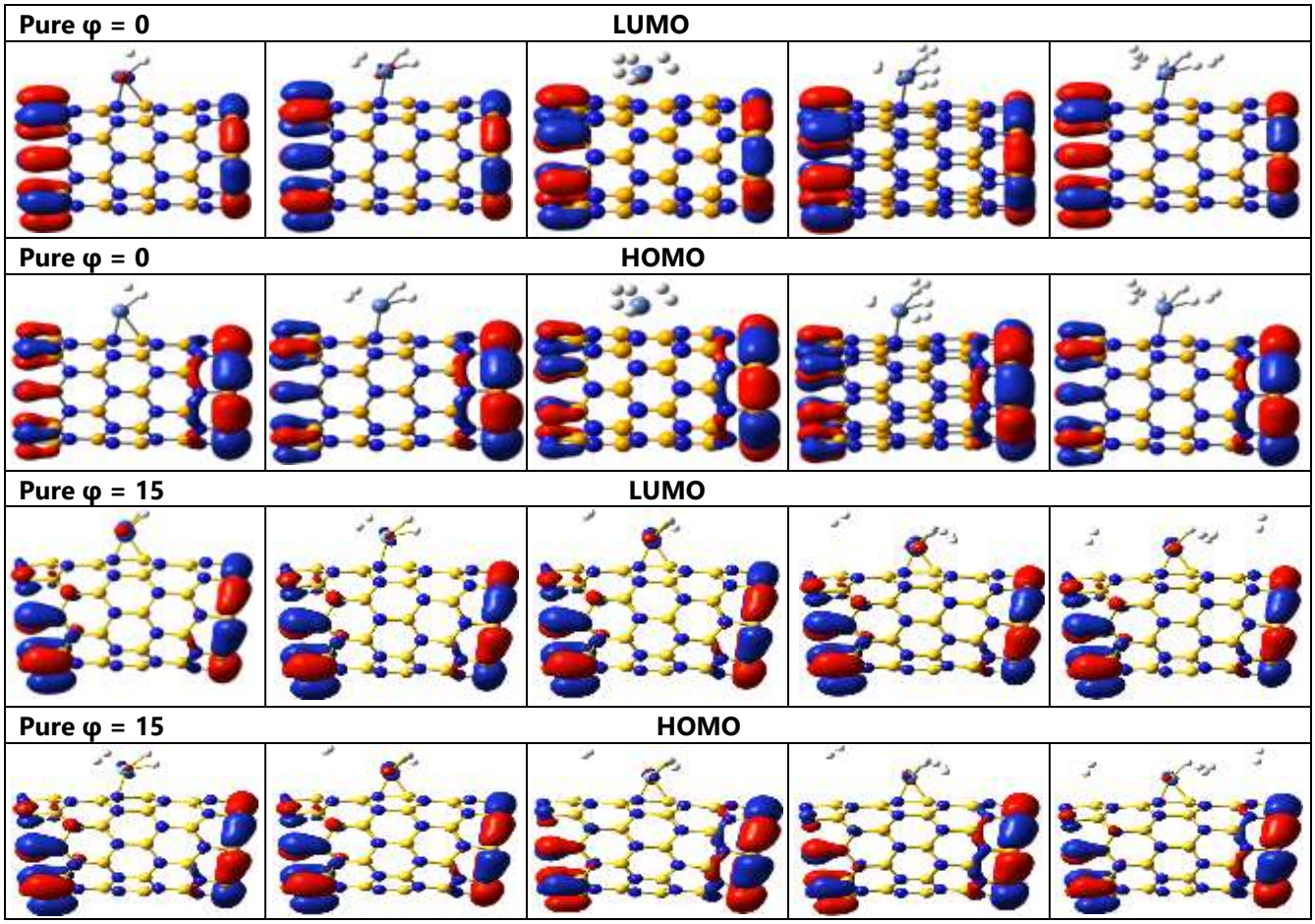

Figure 7. Frontier orbital isosurface plots of nH_2-Ni-N_{40}-B_{40}-φ =0 & 15 (n = 1– 5) complexes.

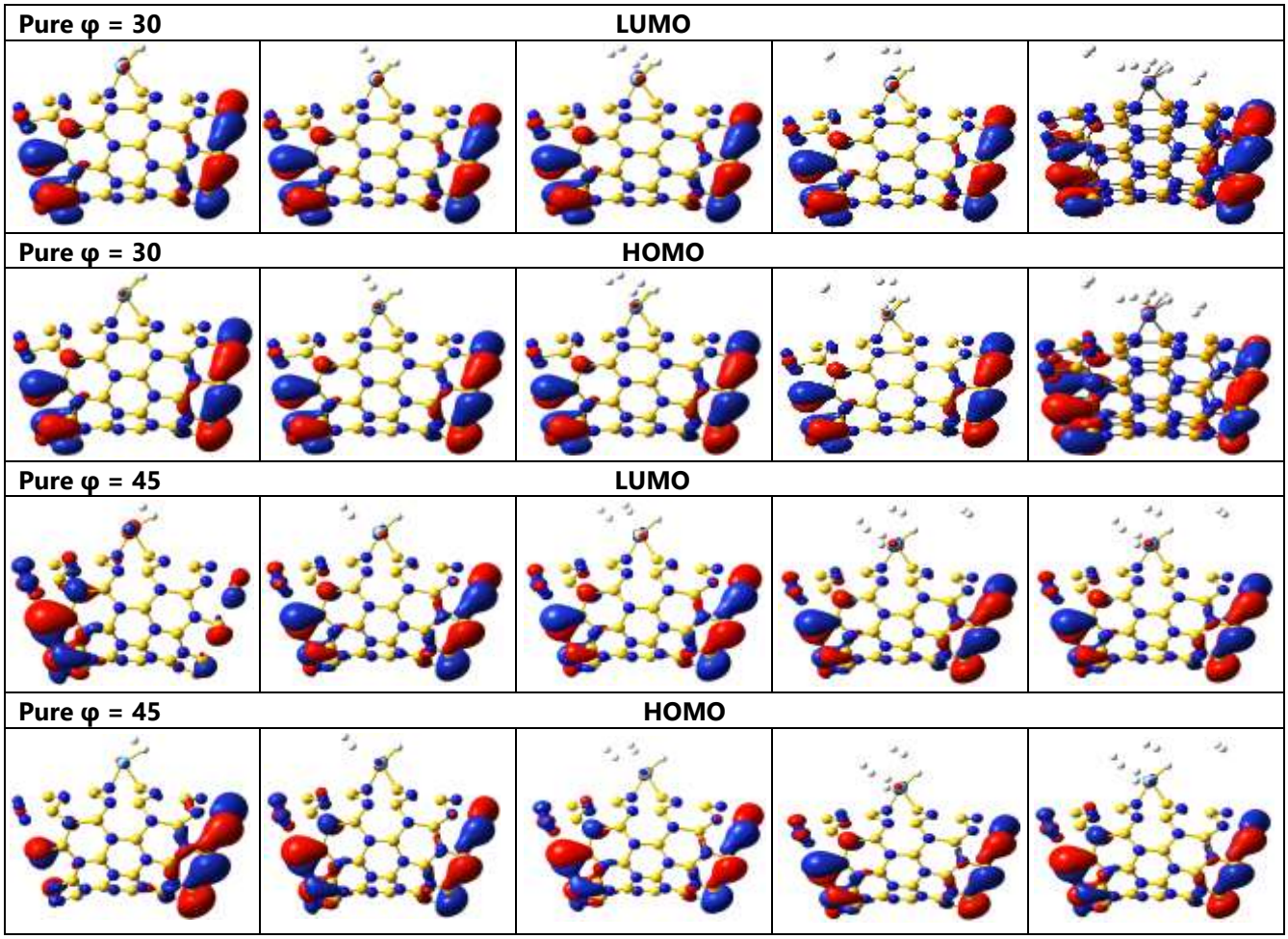

Figure 8. Frontier orbital isosurface plots of nH_2-Ni-N_{40}-B_{40}-φ =30 & 45 (*n* = 1– 5) complexes.

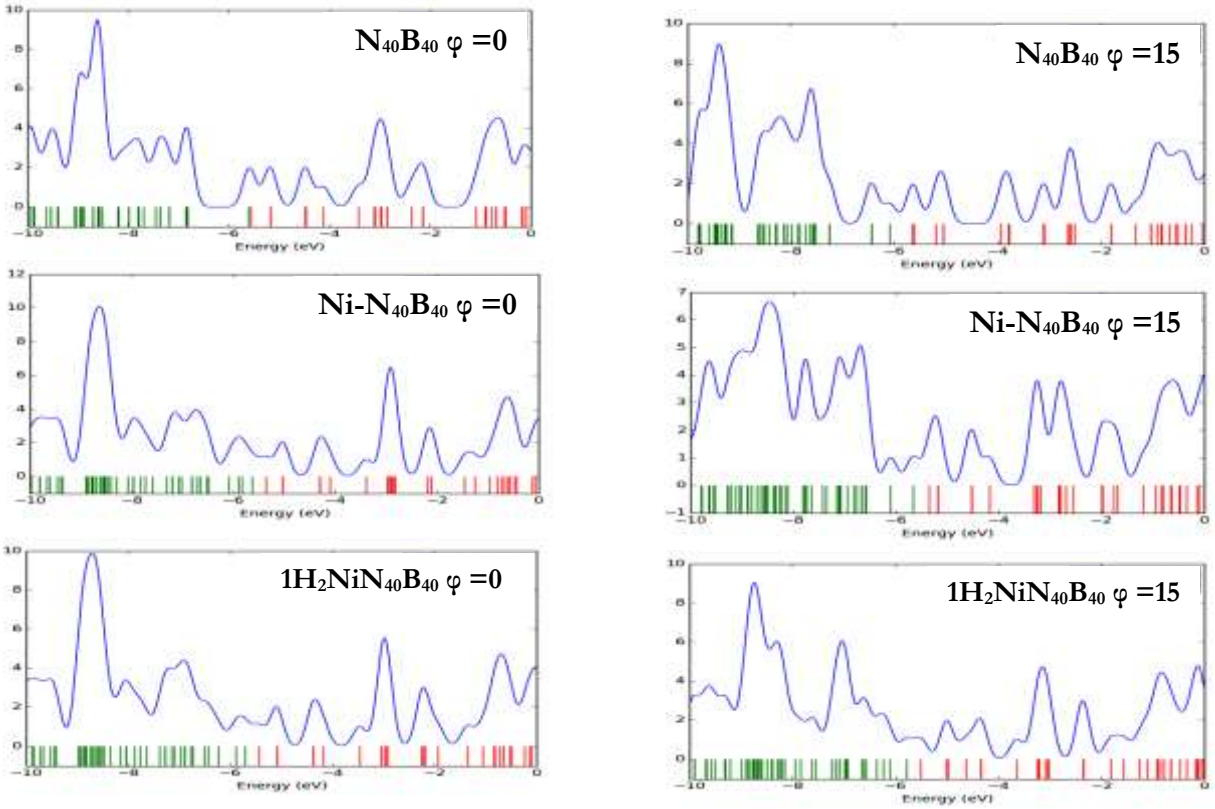

Figure 9. Density of states (DOS) of nH_2-Ni-$N_{40}B_{40}$-φ =0, 15 (n = 1) complexes.

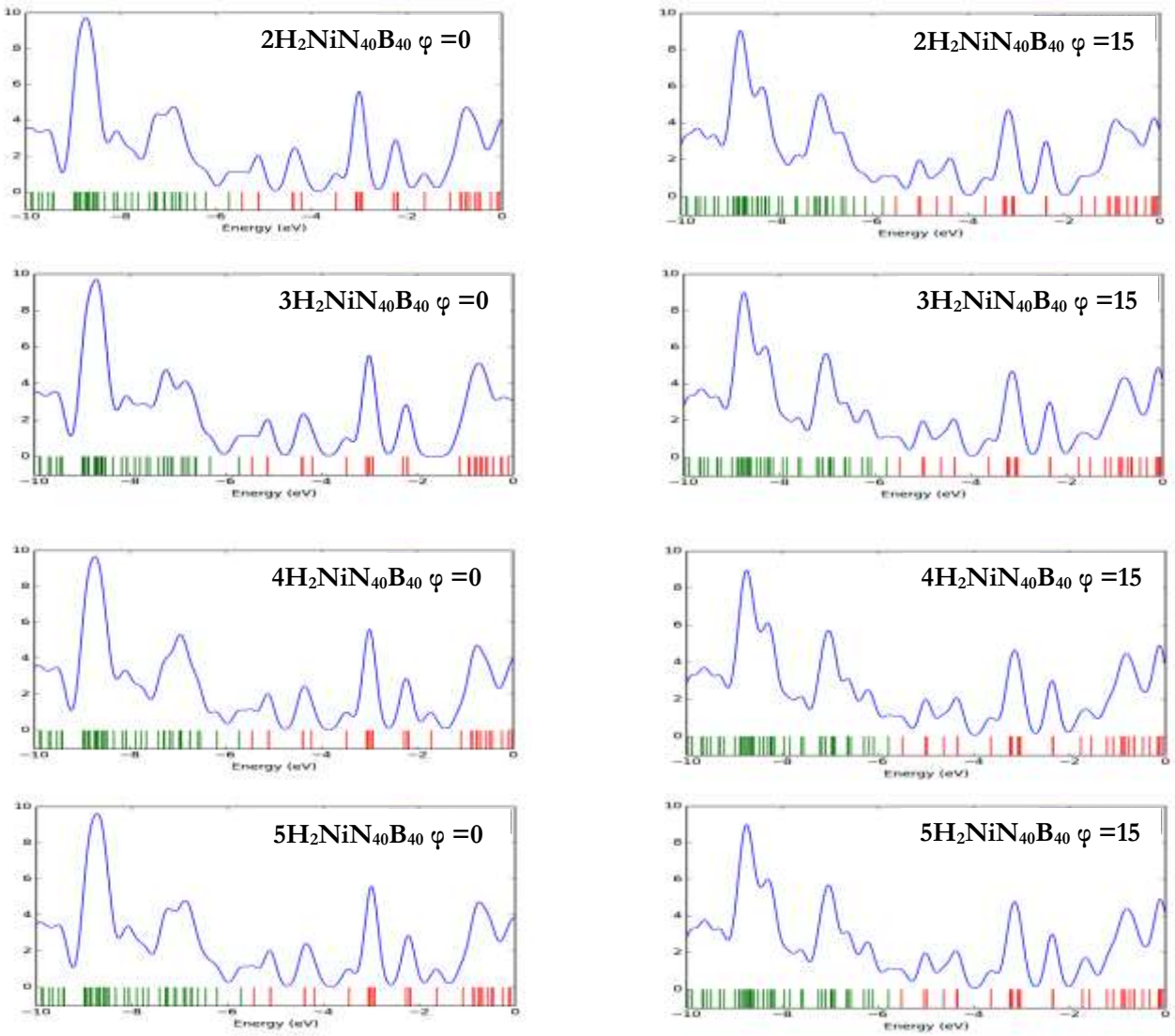

Continue Figure 9. **Density of states (DOS) of nH_2-Ni-$N_{40}B_{40}$-φ =0, 15 (n = 1) complexes.**

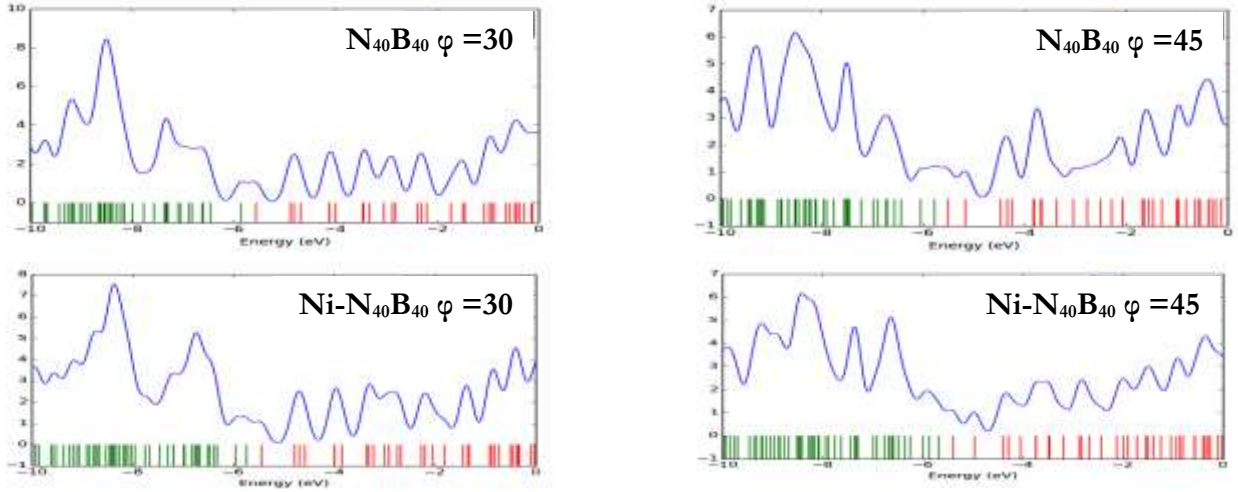

Figure 10. **Density of states (DOS) of nH_2-Ni-$N_{40}B_{40}$-φ =30, 45 complexes.**

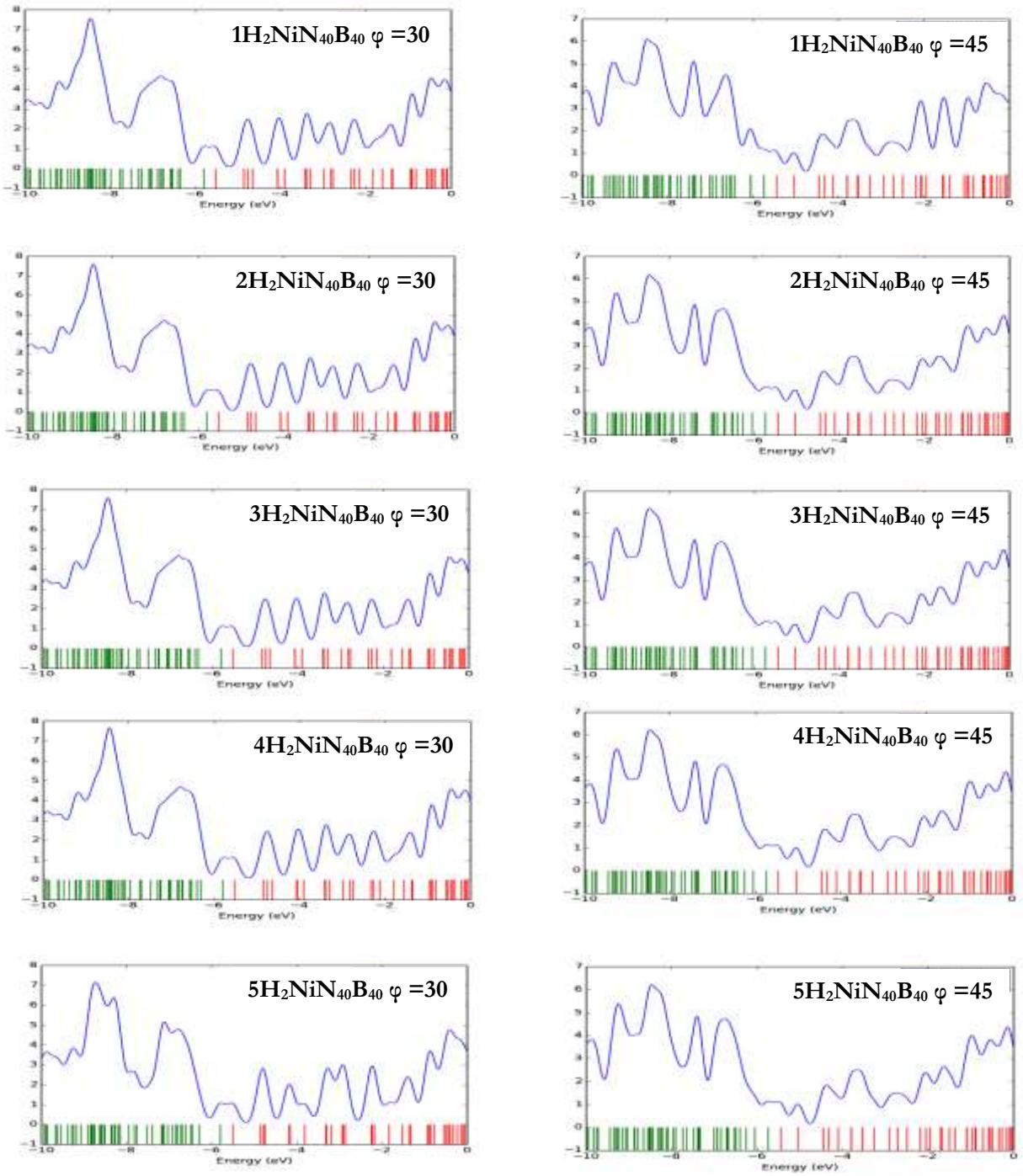

Continue Figure 10. Density of states (DOS) of nH_2-Ni-$N_{40}B_{40}$-φ =30, 45 complexes.

3.3.2. Pairwise and non-pairwise additivities

While the concept of non-additivity has been studied for atom clusters, insulators, and SWCNTs **[58, 59]**, it seems to be overlooked for BNNT. We define the interaction energy $\mathrm{E(i)(BNNT-Ni-nH_2)}$ among three subsystems, the BNNT ($N_{40}B_{40}$), the metal (Ni), and the (nH_2) molecules as

$$\boldsymbol{E(i)(BNNT-Ni-nH_2)=E(BNNT-Ni-nH_2)-E(BNNT)-E(Ni)-E(nH_2)}, \qquad (3)$$

where every energy on the right-hand side of Equation **(3)** is calculated using geometrical parameters corresponding to the equilibrium geometry of $BNNT-Ni-nH_2$ and $E(i)(BNNT-Ni-nH_2)$ Is the energy

required to separate three subsystems without changing their geometrical parameters. This energy can be decomposed into three pairwise components and a non-additive term$\epsilon^{(\mathrm{nadd})}$; and no geometrical relaxation is allowed within a subsystem

$$\boldsymbol{E_{(i)}(BNNT-Ni-nH_2)=E_{(i)}(BNNT-Ni)+E_{(i)}(BNNT-nH_2)+E_{(i)}(Ni-nH_2)+\epsilon^{(nadd)}} \quad (4)$$

where

$$\boldsymbol{E_{(i)}(A..B)=E(A..B)-E(A)-E(B)(A\neq B)=BNNT,Ni,nH_2} \quad (5)$$

The non-additivity $\epsilon^{(nadd)}$ term **[60]** is a measure of cooperative interactions among the subsystems, where

$$\boldsymbol{E_{(i)}(BNNT-Ni)=E(BNNT-Ni)-E(BNNT)-E(Ni)} \quad (6)$$

$$\boldsymbol{E_{(i)}(BNNT-nH_2)=E(BNNT-nH_2)-E(BNNT)-E(nH_2)} \quad (7)$$

$$\boldsymbol{E_{(i)}(Ni..nH_2)=E(Ni..nH_2)-E(Ni)-E(nH_2)} \quad (8)$$

$$\boldsymbol{\epsilon^{(nadd)}=E_{(i)}(BNNT-Ni-nH_2)-E_{(i)}(BNNT-Ni)-(BNNT-nH_2)-E_{(i)}(Ni-nH_2)} \quad (9)$$

In **Table 9** we present total interaction energies of nH_2 - Ni-BNNT-φ =0, (n =4, 5) and for the interactions of nH_2 - Ni-BNNT-φ =15, 30, 45 , (n =2,3) complexes, pairwise additive components, and non-pairwise additive term as defined in **Equations (3)–(9)**. In **Table (9)**, the total interaction energies of $E_{(i)}(BNNT-\mathrm{Ni}-\mathrm{nH_2})$ complexes are seen to be dominated by the pairwise additive component $E_{(i)}(BNNT-Ni)$. An important issue in any study of a support–metal system is the extent to which the support (BNNT) influences the interaction of an adsorbate (nH_2) with the metal (Ni). The $E_{(i)}(BNNT-\mathrm{Ni})$ terms are always greater than the$E_{(i)}(\mathrm{Ni}-\mathrm{nH_2})$ term. This implies that the binding of nH_2 is mostly dominated by the support–metal contribution$E_{(i)}(BNNT-\mathrm{Ni})$, followed by the pairwise metal–dihydrogen additive contribution$E_{(i)}(\mathrm{Ni}-\mathrm{nH_2})$. We may, therefore, conclude that the BNNT support has a considerable effect on the interaction of nH_2 with Ni, and its role is not restricted to supporting the metal. In other words, the adsorption energy of nH_2 depends on the bending effects and the amount of charge transfer of the metal Ni, which in turn depends on the electronegativity of the BNNT support.

Table 9. Interaction energy components of nH_2-Ni- $N_{40}B_{40}$ -φ = 0 (n=4.5) and nH_2-Ni- $N_{40}B_{40}$ -φ = 15, 30, 45 (n=2,3) complexes, total interaction energies $E_{(i)}^{\mathrm{nH_2-Ni-N_{40}B_{40}}}$ pairwise components $E_{(i)}^{\mathrm{Ni-N_{40}B_{40}}}$, $E_{(i)}^{\mathrm{nH_2-N_{40}B_{40}}}$, $E_{(i)}^{\mathrm{nH_2-Ni}}$, and non-additivity term ϵ^{nadd}. All energies are given in eV.

	$E_{(i)}^{\mathrm{nH_2-Ni-N_{40}B_{40}}}$	$E_{(i)}^{\mathrm{Ni-N_{40}B_{40}}}$	$E_{(i)}^{\mathrm{nH_2-N_{40}B_{40}}}$	$E_{(i)}^{\mathrm{nH_2-Ni}}$	ϵ^{nadd}
(φ = 0)					
$4H_2$-Ni- $N_{40}B_{40}$	**-6.139**	**-3.488**	**0.113**	**-3.587**	**0.822**
$5H_2$-Ni- $N_{40}B_{40}$	**-6.140**	**-3.505**	**0.127**	**-3.573**	**0.811**
(φ = 15)					
$2H_2$-Ni- $N_{40}B_{40}$	**-6.234**	**-3.789**	**0.093**	**-3.482**	**0.944**
$3H_2$-Ni- $N_{40}B_{40}$	**-10.719**	**-9.092**	**-4.879**	**-1.805**	**5.057**
(φ = 30)					
$2H_2$-Ni- $N_{40}B_{40}$	**-6.220**	**-4.621**	**0.026**	**-1.778**	**0.153**
$3H_2$-Ni- $N_{40}B_{40}$	**-6.215**	**-4.625**	**0.023**	**-1.774**	**0.160**
(φ = 45)					
$2H_2$-Ni- $N_{40}B_{40}$	**-6.436**	**-4.836**	**0.024**	**-1.868**	**0.243**
$3H_2$-Ni- $N_{40}B_{40}$	**-6.436**	**-4.852**	**0.028**	**-1.949**	**0.336**

3.3.3. MEPs

Molecular electrostatic potential (MEP) contours or surfaces have been established extensively as a guide to the interpretation and prediction of molecular behavior [61]. It has been shown to be a useful tool for studying both electrophilic and nucleophilic processes, in particular, the 'recognition' of one molecule by another [62,63]. Electrostatic interactions play an important role in SWCNT sensor investigations [64, 65]. Despite using different theoretical methodologies, several studies indicate that defect sites on SWCNTs are chemically more reactive than defect-free sites [66–68]. MEPs are either negative, low potentials that are characterized by an abundance of electrons and reactive with electrophiles, or positive, high potentials that are characterized by an absence of electrons and reactive with nucleophiles. We denote the former by deep red colour and the later with a deep blue colour.

The MEP contours of Ni-BNNT and nH_2-Ni/BNNT at φ =0, 15, 30, 45 are given in **Figure 11**. As shown, the intensity of the contours increases noticeably with introducing the Ni and the adsorption of nH_2 molecules. The positivity and negativity MEP contours of the BNNT- φ = 0, 15, 30, 45 are mostly different. However, the MEP contours grow up around the Ni and the nH_2 molecules. The MEPs of the irreversible $4H_2$-Ni-BNNT- φ =0, $2H_2$-Ni-BNNT- φ =15, 30, 45 are different from those of reversible $5H_2$-Ni-BNNT- φ =0, $3H_2$-Ni-BNNT- φ =15, 30, 45. On the other hand, the results indicate that molecular electrostatic potential is capable of characterizing the complexes $4H_2$-Ni-BNNT- φ =0 (n = 4,5) and nH_2-Ni-BNNT- φ =15,30,45(n=2,3) which are representatives of the irreversible and reversible hydrogen storage reactions. In short, the MEP distributions indicate that the $5H_2$-Ni-BNNT- φ =0 and $3H_2$-Ni-BNNT- φ =15,30,45 are the most suitable configurations for hydrogen storage, based on the recommended adsorption energy range.

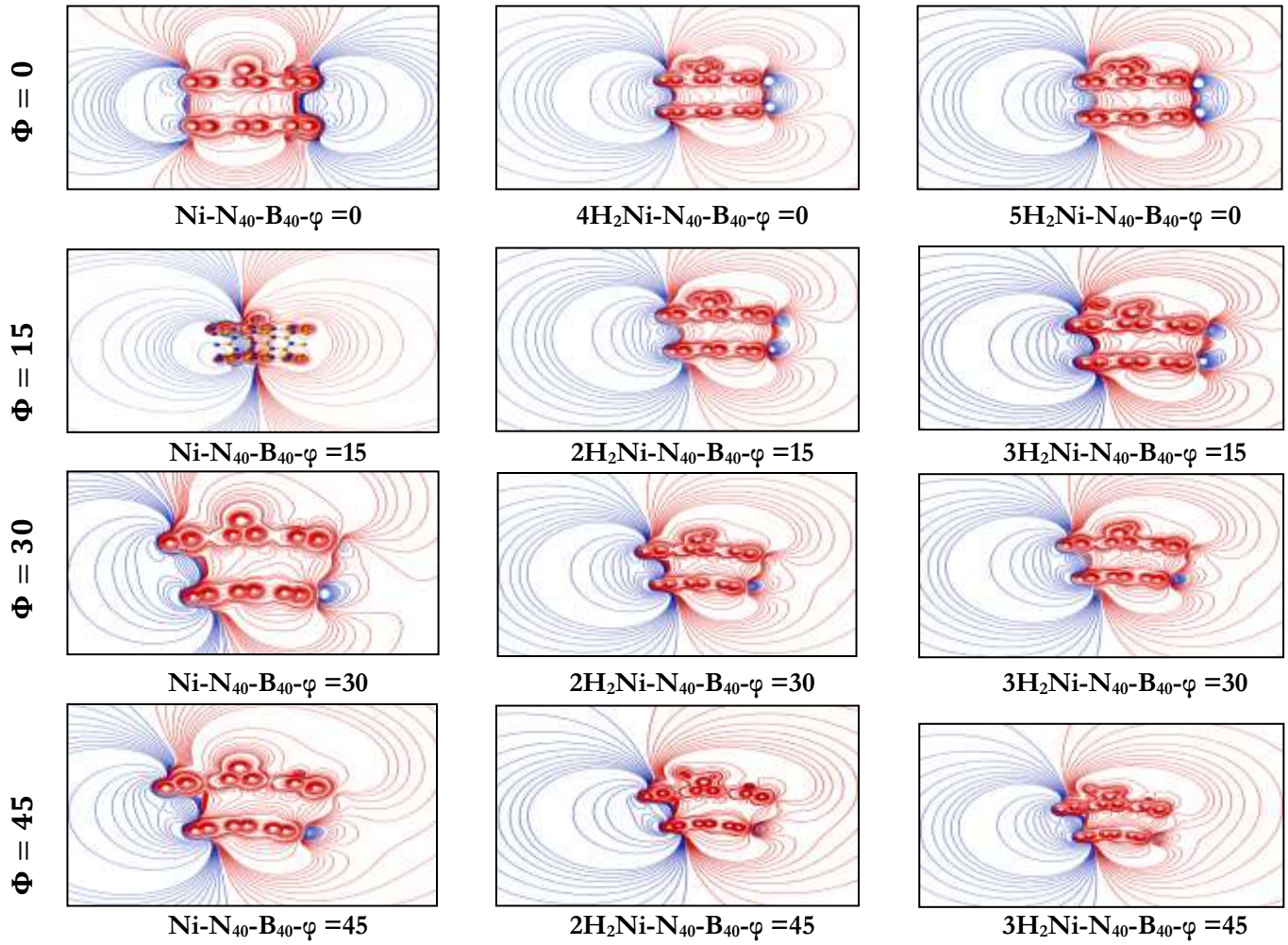

Figure 11. Side views of molecular electrostatic potential surface contours of the Ni-N_{40}-B_{40}-φ =0,15,30,45 and nH_2-Ni-N_{40}-B_{40}-φ =0 (n = 4, 5) complexes and nH_2-Ni-N_{40}-B_{40}-φ =15, 30, 45 (n = 2, 3) complexes.

3.3.4. Electrophilicity

The ionisation potential (IP) and electron affinity (EA) can be calculated from the highest occupied (HOMO) and the lowest unoccupied (LUMO) molecular orbital energies using Koopmans' approximation [69] where $IP = -HOMO$ and $EA = -LUMO$. The chemical potential μ and (χ) are defined as [69]

$$\mu = -\chi = -\frac{IP+EA}{2} \qquad (10).$$

Pearson [70] introduced two parameters 'chemical hardness (η)' and 'chemical softness (S) ' to account for the stability of a molecule. Hardness(η) can also be expressed in terms of HOMO and LUMO, implying a finite difference approach [69], as follows:

$$\eta \approx IP + EA \approx E_{LUMO} - E_{HOMO} \qquad (11)$$

The softness can be defined as [71]

$$S = \frac{1}{2\eta} \qquad (12)$$

The electrophilicity [72-74](ω) is defined as

$$\omega = \frac{\mu^2}{2\eta} = \frac{\chi^2}{2\eta} \qquad (13)$$

Which measures the energy stabilization when the molecule accepts an additional electrical charge from the environment. It is noted that a lower energy gap (Eg) between the LUMO and HOMO of a compound implies a greater and easier possibility of the electron transition between these energy levels. Additionally, a small value of Eg for the compound is an indicator of lower chemical stability. In other words, the respective chemical hardness (η) should be low and electrophilicity (ω), which is a parameter indicating reactivity, should be high.

The ionization potential(IP/eV), electron affinity(EA/eV), chemical hardness (η/eV), electronegativity(χ/eV), softness(S/eV), and electrophilicity (ω/eV) of nH_2 - Ni-BNNT-φ =0, (n =4, 5) and for the interactions of nH_2 - Ni-BNNT-φ =15, 30, 45, (n =2,3) complexes are collected in **Table 10**.

Table 10. The ionisation potential (I/eV), electron affinity (A/eV), chemical hardness (η/ eV), electronegativity (χ/eV), softness(S/eV), and electrophilicity (ω/eV) of nH_2-Ni- $N_{40}B_{40}$ -φ = 0 (n=4.5) and nH_2-Ni- $N_{40}B_{40}$ -φ = 15,30,45 (n=2.3) complexes.

	I	*A*	*η*	*χ*	*S*	*ω*
φ = 0						
$4H_2$ Ni-$N_{40}B_{40}$-φ = 0	**5.726**	**5.453**	**0.273**	**5.590**	**1.832**	**57.221**
$5H_2$ Ni-$N_{40}B_{40}$-φ = 0	**5.721**	**5.451**	**0.270**	**5.586**	**1.852**	**57.784**
φ = 15						
$2H_2$ Ni-$N_{40}B_{40}$-φ = 15	**5.786**	**5.51**	**0.276**	**5.648**	**1.812**	**57.790**
$3H_2$ Ni-$N_{40}B_{40}$-φ = 15	**5.771**	**5.494**	**0.277**	**5.633**	**1.805**	**27.265**
φ = 30						
$2H_2$ Ni-$N_{40}B_{40}$-φ = 30	**5.801**	**5.519**	**0.282**	**5.66**	**1.773**	**56.801**
$3H_2$ Ni-$N_{40}B_{40}$-φ = 30	**5.799**	**5.516**	**0.283**	**5.658**	**1.767**	**56.550**
φ = 45						
$2H_2$ Ni-$N_{40}B_{40}$-φ = 45	**5.737**	**5.454**	**0.283**	**5.596**	**1.767**	**55.317**
$3H_2$ Ni-$N_{40}B_{40}$-φ = 45	**5.738**	**5.455**	**0.283**	**5.597**	**1.767**	**55.337**

The $4H_2$ - Ni-BNNT-φ =0 is characterized by a high value of ionization potential(IP/eV), electron affinity(EA/eV), chemical hardness (η/eV), electronegativity(χ/eV) relative to the $5H_2$-Ni- BNNT-φ = 0. The softness(S/eV), and electrophilicity (ω/eV)of $4H_2$ - Ni-BNNT-φ =0 is slightly smaller than that of the complex $5H_2$ - Ni-

BNNT-φ =0. But the $2H_2$ - Ni-BNNT-φ =15,30 is characterized by a high value of ionization potential(IP/eV), electron affinity(EA/eV), electronegativity(χ/eV), softness(S/eV), and electrophilicity (ω/eV)relative to the $3H_2$-Ni- BNNT-φ = 0. The chemical hardness (η/eV) of $2H_2$ - Ni-BNNT-φ =15,30 are slightly smaller than that of the complex $3H_2$ - Ni-BNNT-φ =15,30. The ionization potential(IP/eV), electron affinity(EA/eV), chemical hardness (η/eV), electronegativity(χ/eV) of the nH_2 - Ni-BNNT-φ =0 (n=4,5) complex is characterized by slightly smaller than that of the nH_2 - Ni-BNNT-φ =15,30 (n=2,3)complex. But the nH_2 - Ni-BNNT-φ =0 (n=4,5) complex is characterized by high value softness(S/eV), and electrophilicity (ω/eV)relative to the nH_2-Ni-BNNT-φ = 15,30 (n=2,3) complex. A good electrophile will be characterized by a high value of electrophilicity (ω). It is, therefore, evident that while the complex nH_2-Ni- BNNT-φ = 0 is a better electrophile than nH_2-Ni-BNNT-φ = 15,30, it is slightly more stable and less reactive than nH_2-Ni- BNNT-φ = 15,30 complex.

3.3.5. Spectral analysis

The numerical harmonic vibrational analysis of the simulated IR spectrum was carried out to find the strongest vibrational modes of molecular hydrogen interactions with Ni-BNNT. The modes that are mixed with H_2 vibrations were not taken into account, and the calculated IR bands, force constants, and dipole strength for $4H_2$-Ni- BNNT-φ = 0,15,30,45 complexes are collected in **Table 11**.

Table 11. Infrared(IR),Raman(R),P-and U-depolarization spectra of H_2(H(82)-H(83) , H(84)-H(85) , H(86)-H(87), H (88)-H (89)) of nH_2-Ni- $N_{40}B_{40}$ -φ = 0 (n=4.5) and nH_2-Ni- $N_{40}B_{40}$ -φ = 15,30,45 (n=2,3) complexes in the gas phase calculated at the B3LYP/6-31g(d,p) level of theory.

		Infrared			Raman		
		Frequency (Cm^{-1})	Force constant mDyne/A)	Dipole strength (10^{-40} esu^2 Cm^2)	Scattering activity (A^4/AMU)	P-depol.	U-depol.
φ = 0							
$4H_2$ Ni-$N_{40}B_{40}$-φ = 0	H(82)-H(83)	2281.227	3.123	502.077	1014.033	0.349	0.518
	H(84)-H(85)	4460.407	11.814	2.745	60.661	0.202	0.336
	H(86)-H(87)	4471.328	11.872	2.788	65.573	0.212	0.349
	H(88)-H(89)	3384.600	6.807	165.784	681.562	0.356	0.525
$5H_2$ Ni-$N_{40}B_{40}$-φ = 0	H(82)-H(83)	2377.714	3.384	412.831	493.024	0.373	0.544
	H(84)-H(85)	4445.562	11.735	0.342	451.924	0.350	0.518
	H(86)-H(87)	4460.581	11.815	0.374	283.338	0.371	0.541
	H(88)-H(89)	4463.595	11.831	0.304	259.614	0.351	0.520
	H(90)-H(91)	3176.925	6.001	232.533	427.231	0.340	0.508
φ = 15							
$2H_2$ Ni-$N_{40}B_{40}$-φ = 15	H(82)-H(83)	2477.799	3.668	318.262	374.409	0.382	0.553
	H(84)-H(85)	3096.560	5.702	402.816	923.837	0.345	0.513
$3H_2$ Ni-$N_{40}B_{40}$-φ = 15	H(82)-H(83)	2694.194	4.327	1660.53	19788.175	0.338	0.506
	H(84)-H(85)	4474.404	11.888	8.073	89.131	0.140	0.246
	H(86)-H(87)	4444.900	11.732	2.004	149.154	0.249	0.399
φ = 30							
$2H_2$ Ni-$N_{40}B_{40}$-φ = 30	H(82)-H(83)	4452.179	11.770	2.847	108.603	0.245	0.394
	H(84)-H(85)	2798.866	4.666	964.208	3842.028	0.348	0.516
$3H_2$ Ni-$N_{40}B_{40}$-φ = 30	H(82)-H(83)	2800.830	4.672	968.464	4091.223	0.347	0.516
	H(84)-H(87)	4455.538	11.788	0.678	104.133	0.283	0.441
	H(85)-H(86)	4453.121	11.775	2.716	48.725	0.142	0.248
φ = 45							
$2H_2$ Ni-$N_{40}B_{40}$-φ = 45	H(82)-H(83)	2892.167	5.013	896.97	3354.281	0.361	0.531
	H(84)-H(85)	4294.885	10.953	42.178	1488.146	0.352	0.520
$3H_2$ Ni-$N_{40}B_{40}$-φ = 45	H(82)-H(83)	2902.922	5.022	873.646	3505.145	0.361	0.530
	H(84)-H(85)	4323.478	11.100	25.037	1223.409	0.356	0.525
	H(86)-H(87)	4419.649	11.599	7.806	817.249	0.388	0.559

Inspection of (IR) frequencies shows that all the bands undergo changes in position and intensities following the bending deformation effects. An upshift of the band of frequency (2281.227 – 2377.714 cm^{-1}) assigned to H_2 in $4H_2$-Ni- BNNT-φ = 0 with force constant (3.123 m Dyne A^{-1}) and dipole strength (502.077x 10^{-40} esu^2 Cm^2) is observed under the effect of the addition of one extra hydrogen molecule in $5H_2$-Ni- BNNT-φ = 0. This is followed by down shift of Raman (R) scattering activity (1014.033 – 493.024 A^4 AMU^{-1}), and upshifts of P-depolarization (0.349 – 0.373), and U-depolarization (0.518 – 0.544). While for $2H_2$-Ni- BNNT-φ = 15 and upshift of the band of frequency (2477.799 – 2694.194 cm^{-1}) assigned to H_2 with force constant (3.668 m Dyne A^{-1}) and dipole strength (318.262x$10^{-40}$$esu^2$ Cm^2) is observed under the effect of the addition of one extra hydrogen molecule in $3H_2$-Ni- BNNT-φ = 15. This is followed by upshift of Raman (R) scattering activity (374.409 – 19788.175 A^4 AMU^{-1}) and downshifts of P-depolarization (0.382 – 0.338), and U-depolarization (0.553 – 0.506). While for $2H_2$-Ni- BNNT-φ = 30 a downed shift of the band of frequency (4452.179 – 2800.830 cm^{-1}) assigned to H_2 with force constant (11.770 m Dyne A^{-1}) and dipole strength (2.847 x10^{-40} esu^2 Cm^2) is observed under the effect of the addition of one extra hydrogen molecule in $3H_2$-Ni- BNNT-φ = 30. This is followed by upshift of Raman (R) scattering activity (108.603 – 4091.223 A^4 AMU^{-1}), P-depolarization (0.245 – 0.347), and U-depolarization (0.394– 0.516). While for $2H_2$-Ni- BNNT-φ = 45 and upshift of the band at frequency (2892.167– 2902.922 cm^{-1}) assigned to H_2 with force constant (5.013 m Dyne A^{-1}) and dipole strength (896.97x10^{-40} esu^2 Cm^2) is observed under the effect of the addition of one extra hydrogen molecule in $3H_2$-Ni- BNNT-φ = 45. This is followed by upshift of Raman (R) scattering activity (3354.281– 3505.145 A^4 AMU^{-1}). The deformed $4H_2$-Ni-BNNT-φ =30 structure exhibits higher infrared frequency and force constant, than those of the un-deformed and deformed $4H_2$-Ni-BNNT-φ =0, 15, 45. However, the deformed structure φ =30 exhibits lower scattering activity and higher P- and U depolarization than those of the un-deformed and deformed $4H_2$-Ni-BNNT-φ =0, 15, 45. This indicates that IR and R spectral parameters characterize the deformed structure φ =30 structure for which H_2 binding energy (-0.249 eV) is in the recommended energy range for hydrogen storage, to be energetically more preferable than the deformed structure φ =15, 45. These effects are attributed to the interaction between H_2 molecules and the Ni atom deposited on the BNNT-φ = 0,15,30,45. On the other hand, the results indicate that (IR) and (R) spectral parameters are capable of characterizing the complexes $4H_2$-Ni- BNNT-φ = 0 and $2H_2$-Ni- BNNT-φ = 15, 30, 45 which are representatives of the irreversible and $5H_2$-Ni- BNNT-φ = 0 and $3H_2$-Ni- BNNT-φ = 15, 30, 45 are representatives of reversible hydrogen storage reactions.

4. Conclusion

In summary, we have performed DFT calculations to investigate the mechanical bending effects on hydrogen storage of Ni decorated (8, 0) BNNTs under different bending angles. Based on the current results, physisorption, gravimetric capacity properties of hydrogen storage reactions meet the ultimate targets of DOE for practical applications. Two types of reactions, namely reversible and irreversible, were characterized in terms of DOS, pairwise and non-pairwise additivities, IR, R, electrophilicity, and MEPs. All of the adsorption reactions are exothermic. In the ideal circumstances, there is no evidence for metal clustering and the hydrogen storage capacity is, therefore, expected to be as large as 5.691 wt%. While the desorption activation barriers of the complexes nH_2-Ni-BNNT-φ =0 (n = 1-4) and nH_2-Ni-BNNT-φ =15,30,45 (n = 1-2)) are outside the Department of Energy domain (-0.2 to -0.6 eV), the complexes nH_2-Ni-BNNT-φ =0 (n = 5) and nH_2-Ni-BNNT-φ =15,30,45 (n = 3-5). We hope that the present calculations suggest an approach to characterize and engineer new nanostructured materials for hydrogen storage.

References

[1]E. Durgun, S. Ciraci, and T. Yildirim, Fictionalization of carbon-based nanostructures with light transition-Metal atoms for hydrogen storage, Phys. Rev. B., **77**, 085405, (2008).

[2] J.R. Cheng, L.B. Zhang, R. Ding, Z.F. Ding, X. Wang, and Z. Wang, Grand canonical Monte Carlo simulation of hydrogen physisorption in single-walled boron nitride nanotubes, Int. J. Hydrogen Energy., **32**,3402, (2007).

[3] C. Liu, Y.Y. Fan, M. Liu, H.T. Cong, H.M. Cheng, and M.S. Dresselhaus, Hydrogen Storage in Single-Walled Carbon Nanotubes at Room Temperature Science., **286**, 1127, (1999).

[4] G.K. Dimitrakakis, E. Tylianakis, and G.E. Froudakis, Pillared Graphene: A New 3- D Network Nanostructure for Enhanced Hydrogen Storage, Nano Lett., **8**, 3166, (2008).

[5] S. Iijima, Helical microtubules of graphitic carbon, Nature.,**354**, 56 ,(1991).

[6] D. Golberg, Y. Bando, C.C. Tang, and C.Y. Zhi, Boron Nitride Nanotubes, Adv. Mater., **19**, 2413, (2007).

[7] A. Rubio, J.L. Corkill, and M.L. Cohen, Theory of graphitic boron nitride nanotubes, Phys. Rev. B., **49**, 5081, (1994).

[8] N.G. Chopra, R.J. Luyken, K. Cherrey, V.H. Crespi, M.L. Cohen, S.G. Louie, and A. Zettl, Boron Nitride Nanotubes, Science., **269**, 966 (1995).

[9] X. Blase, A. Rubio, S.G. Louie, and M.L. Cohen, Stability and Band Gap Constancy of Boron Nitride Nanotubes, Euro phys. Lett., **28**, 335 (1994).

[10] A. Loiseau, F. Willaime, N. Demoncy, G. Hug, and H. Pascard, Boron Nitride Nanotubes with Reduced Numbers of Layers Synthesized by Arc Discharge, Phys. Rev. Lett., **76**, 4737, (1996).

[11] E. Bengu, and L.D. Marks, Single-Walled BN Nanostructures, Phys. Rev. Lett., **86**, 2385,(2001).

[12] V. Nirmala, P. Kolan daivel, Structure and electronic properties of armchair boron nitride nanotubes, J. Mol. Struct. (THEOCHEM)., **817**, 137, (2007).

[13] J. Chen, and F. Wu, Review of hydrogen storage in inorganic fullerene-like nanotubes, Appl. Phys. A-Mater., **78**, 989, (2004).

[14] R.Z. Ma, Y. Bando, H.W. Zhu, T. Sato, C.L. Xu, and D.H. Wu, J. Am. Chem. Soc., **124**, 7672, (2002).

[15] J. Cheng, R. Ding, Y. Liu, Z. Ding, and L. Zhang, Computer simulation of hydrogen physisorption in single-walled boron nitride nanotube arrays, Computational Materials Science.,**40**, 341, (2007).

[16] J. X. Zhao, and Y.H. Ding, The effects of O_2 and H_2O adsorbates on field- emission properties of an (8, 0) boron nitride nanotube: a density functional theory study, Nanotechnology., **20**, 085704,(2009).

[17] J. H. Yuan, and K. Liew, Effects of boron nitride impurities on the elastic properties of carbon nanotubes, Nanotechnology., **19**, 445703,(2008).

[18] G. Mpourmpakis, and G.E. Froudakis, Why boron nitride nanotubes are preferable to carbon nanotubes for hydrogen storage?: An *ab initio* theoretical study, Catal Today., **120**, 341, (2007).

[19] B. Baumeier, P. Kruger, and J. Pollmann, Structural, elastic, and electronic properties of SiC, BN, and BeO nanotubes, Phys. Rev. B., **76**, 085407, (2007).

[20] C.C. Tang, Y. Bando, X.X. Ding, S.R. Qi, and D. Golberg, Catalyzed Collapse and Enhanced Hydrogen Storage of BN Nanotubes, J. Am. Chem. Soc., **124**, 14550,(2002).

[21] X.J. Wu, J. L. Yang, J.G. Hou, and Q.S. Zhu, Deformation-induced site selectivity for hydrogen adsorption On boron nitride nanotubes Phys. Rev. B., **69**, 153411, (2004).

[22] S.P. Ju, Y.C. Wang and T.W. Lien, Tuning the electronic properties of boron nitride nanotube by Mechanical uni-axial deformation: a DFT study, Nanoscale Res. Lett., **6**, 160, (2011).

[23] G.G. Wildgoose, E.C. Banks, and G.R. Compton, Metal Nanoparticles and Related Materials Supported on Carbon Nanotubes: Methods and Applications Small., **2**, 182, (2006).

[24] Q.W. Han, and A. Zettl, Functionalized Boron Nitride Nanotubes with a Stannic Oxide Coating: A Novel Chemical Route to Full Coverage J. Am. Chem. Soc., **125**, 2062, (2003).

[25] Y.C. Zhi, Y. Bando, C. Tang, and D. Golberg, Purification of Boron Nitride Nanotubes through Polymer Wrapping J. Phys. Chem. B. **110**, 1525, (2006).

[26] T. Sainsbury, T. Ikuno, D. Okawa, D. Pacile, J.M.J. Frechet, and A. Zettl, Self-Assembly of Gold Nanoparticles At the Surface of Amine- and Thiol-Functionalized Boron Nitride Nanotubes, J. Phys. Chem. C., **111**, 12992, (2007).

[27] H.W. Shin, H.S. Yang, A.W. Goddard, and. J. Kang, Ni-dispersed fullerenes: Hydrogen storage and Desorption properties, Appl. Phys. Lett., **88**, 053111, (2006).
[28] J.X. Wu, and C.X. Zeng, Adsorption of transition-metal atoms on boron nitride nanotube: A density-functional study J. Chem. Phys., **125**, 044711 (2006).
[29] J.X. Wu, L. J. Yang, and C.X. Zeng, Adsorption of hydrogen molecules on the platinum-doped boron nitride nanotubes J. Chem. Phys., **125**, 044704, (2006).
[30] S.L. Hu, E.J. Kan, and J.L. Yang, First-principles study of the interaction between H_2 molecules and BN nanotubes with BN divacancies J. Chem. Phys., **127**, 164718, (2007).
[31] X.J. Wu, J.L. Yang, J.G. Hou, and Q.S. Zhu, Defects-enhanced dissociation of H_2H_2 on boron nitride nanotubes, J. Chem. Phys., **124**, 054706,(2006).
[32]A. Shevlin and Z.X. Guo, Hydrogen sorption in defective hexagonal BN sheets and BN nanotubes, Phys. Rev. B., **76**, 024104, (2007).
[33] T. Terao, Y. Bando, M. Mitome, K. Kurashima, C.Y. Zhi, C.C. Tang, and D. Golberg, Effective synthesis of surface-modified boron nitride nanotubes and related nanostructures and their hydrogen uptake, Physica E., **40**, 2551, (2008).
[34] R.J. Baierle, P. Piquini, T.M. Schmidt, and S.J. Fazzio, Hydrogen Adsorption on Carbon-Doped Boron Nitride Nanotubem Phys. Chem. B., **110**, 21184, (2006).
[35] F. Li, Y. Xia, M. Zhao, X. Liu, B. Huang, and Y. Ji, C. Song, Theoretical study of hydrogen atom adsorbed on carbon-doped BN nanotubes, Phys. Lett. A., **357**, 369, (2006).
[36] E. Durgun, Y.R. Jang, and S. Ciraci, the Hydrogen storage capacity of Ti-doped boron- nitride and B/Be-substituted carbon nanotubes, Phys. Rev. B., **76** , 073413, (2007).
[37] N. Arzate, R. A. Va'zquez-Nava, and J. E. Mej'ı'a, Linear optical response of (6,0) boron nitride nanotubes Adsorbed with molecular hydrogen Phys. Stat. Sol. C., **5**, 2595, (2008).
[38] J X Zhao, Y H Ding, Theoretical Study of Ni Adsorption on Single-Walled Boron Nitride Nanotubes with Intrinsic Defects, J Phys Chem C., **112**, 5778, (2008).
[39] L.P. Zhang, P. Wu, and M.B. Sullivan, Hydrogen Adsorption on Rh, Ni, and Pd Functionalized Single-Walled Boron Nitride Nanotubes J. Phys. Chem. C.,**15**, 4289, (2011).
[40] W. Lei, H. Zhang, Y. Wu, B. Zhang, D. Liu, S. Qin, Z. Liu, L. Liu, Y. Ma and Y. Chen, Oxygen-doped boron nitride nanosheets with excellent performance in hydrogen storage, Nano Energy., **6**, 219, (2014).
[41] Y. Liu, W. Liu, R. Wang, L. Hao, and W. Jiao, Hydrogen storage using Na-decorated graphyne and its boron Nitride analog, Int. J. Hydrogen Energy., **39**, 12757, (2014).
[42] Becke AD. Density-functional thermochemistry. III. The role of exact exchange. J Chem Phys., **98**, 5648, (1993).
[43] Vosko SH, Wilk L, Nusair M. Accurate spin-dependent electron liquid correlation energies for local spin Density calculations: a critical analysis. Can J Phys., **58**, 1200, (1980).
[44] Becke AD. Density-functional exchange-energy approximation with correct asymptotic behavior. Phys Rev., **38**, 3098, (1988).
[45] Lee C, Yang W, Parr RG. Development of the Colle-Salvetti correlation-energy formula into a functional of The electron density. Phys Rev B., **37**, 789, (1988).
[46] R. Caballol, O. Castell, F. Illas, J.P. Malrieu, and I.P.R. Moreira, Remarks on the Proper Use of the Broken Symmetry Approach to Magnetic Coupling J. Phys. Chem. A., **101**, 7860,(1997).
[47] Ricca A, Bauschlicher CW. Successive binding energies of $Fe(CO)^{5+}$. J Phys Chem., **98**, 12899, (1994).
[48] Russo TV, Martin RI, Hay PJ. Application of gradient corrected density functional theory to the structures And the rmochemistries of ScF_3, TiF_4, VF_5, and CrF_6. J Chem Phys., **102**, 8023, (1995).
[49] Siegbahn PE, Crabtree RH. Mechanism of C-H activation by diiron methane monooxygenases: quantum Chemical studies. J Am Chem Soc., **119**, 3103, (1997).
[50] W.R. Duncan, W. Stier, and O.V. Prezhdo, in Nanomaterials: Design and Simulation, edited by P.B. Balbuena and J. M. Semiinario (Elsevier BV, Amsterdam, 2007).
[51] M.J. Frisch, G.W. Trucks, H.B. Schlegel, G.E. Scuseria, M.A. Robb, J.R. Cheeseman, G. Scalmani, V. Barone, B. Mennucci, G.A. Petersson, H. Nakatsuji, M. Caricato, X. Li, H.P. Hratchian, A.F. Izmaylov, J. Bloino, G. Zheng, J.L. Sonnenberg, M. Hada, M. Ehara, K. Toyota, R. Fukuda, J. Hasegawa, M. Ishida, T. Nakajima, Y. Honda, O.

Kitao, H. Nakai, T. Vreven, J.A. Montgomery, Jr., J.E. Peralta, F. Ogliaro, M. Bearpark, J.J. Heyd, E. Brothers, K.N. Kudin, V.N. Staroverov, T. Keith, R. Kobayashi, J. Normand, K. Raghavachari, A. Rendell, J.C. Burant, S.S. Iyengar, J. Tomasi, M. Cossi, N. Rega, J.M. Millam, M. Klene, J.E. Knox, J.B. Cross, V. Bakken, C. Adamo, J. Jaramillo, R. Gomperts, R.E. Stratmann, O. Yazyev, A.J. Austin, R. Cammi, C. Pomelli, J.W. Ochterski, R.L. Martin, K. Morokuma, V.G. Zakrzewski, G.A. Voth, P. Salvador, J.J. Dannenberg, S. Dapprich, A.D. Daniels, O. Farkas, J.B. Foresman, J.V. Ortiz, J. Cioslowski, and D.J. Fox, *Gaussian 09,Revision D.01* (Gaussian, Inc., Wallingford, CT, 2010).

[52] O'Boyle NM, Tenderholt AL, Langner KM. cclib: a library for package-independent computational Chemistry algorithms. J Comput Chem., **29**, 839, (2008).

[53] S. N. Venkataramanan, M. Khazaei, R. Sahara, H. Mizuseki, and Y. Kawazoe, First-principles study of hydrogen storage over Ni and Rh doped BN sheets, Chem. Phys., **359**, 173,(2009).

[54] W. Auwarter, J.T. Kreutz, T. Greber, Osterwalder, XPD and STM investigation of hexagonal boron nitride on Ni(111), J. Surf. Sci., **429** , 229,(1999).

[55] R.D. Lide, editor. CRC handbook of chemistry and physics. 84th ed. Boca Raton: CRC Press LLC; 2003–2004.

[56] K. Fukui, Role of Frontier Orbitals in Chemical Reactions, Science., 218, 747, (1982).

[57] R.S. Ashraf, and E. Klemm. Synthesis and properties of poly (heteroaryleneethynylene)s consisting of electron-accepting benzothiadiazole/ quinoxaline units and electron-donating alkyl thiophene units J. Polym. Sci. A., **43**, 6445, (2005).

[58] A.S. Shalabi, A.M. El Mahdy, and H.O. Taha, Theoretical characterization of axial deformation effects on Hydrogen storage of Ti decorated armchair (5,5), SWCNT Mol. Phys., **111**, 661, (2013).

[59] A.S. Shalabi, A.M. El Mahdy, K.A. Soliman, and H.O. Taha, Theoretical characterisation of irreversible and reversible hydrogen storage reactions on Ni- doped C_{60} fullerene Mol. Phys., **112**, 3057, (2014).

[60] N. Lopez, F. Illas, N. Rosch, and G. Pacchioni, Adhesion energy of Cu atoms on the MgO(001) surface J. Chem. Phys., **110**, 4873, (1999).

[61] D.L. Wang, H.T. Shen, H.M. Gu, and Y.C. Zhai, *Ab initio* studies on the molecular electrostatic potential of C_{50} J. Mol. Struct., **776**, 47, (2006).

[62] G. Naray- Szabo, and G.G. Ferenczy, Molecular Electrostatics Chem. Rev., **95**, 829, (1995).

[63] J.S. Murray, P. Politzer, in A.M. Space (Ed.), Molecular Orbital Calculations for Biological Systems, Oxford University Press, New York, 1998, p. 49, Chapter 3.

[64] X. Wang, X. Li, and H. Li, First-principles study of Eu doped carbon nanotubes Phys. Lett., A. **372**, 6677, (2008) .

[65] K. Parikh, K. Cattanach, R. Rao, D.S. Suh, A. Wu, and S.K. Manohar, Flexible vapour sensors using single walled carbon nanotubes Sens. Actuators B., **113**, 55, (2006).

[66] D. Wang, X. Sun, G. Xin, and D. Hou, *Ab initio* and density functional study on the molecular electrostatic the potential of C_{32} Physica B., **405**, 2745, (2010).

[67] K. Ragavachari, B. Zhang, J.A. Pople, B.G. Johnson, and P.M.W. Gill, Isomers of C_{24}. Density functional Studies including gradient corrections Chem. Phys. Lett., **220**, 385, (1994).

[68] P. Politzer, and D.G. Truhlar, Chemical Applications of Atomic and Molecular Electrostatic Potentials, Plenum, New York, 1981.

[69] R. G. Parr and W. Yang, Density Functional Theory of Atoms and Molecules. Oxford University Press, New York. (1989)

[70] R.G. Pearson, Hard and Soft Acids and Bases. Dowden, Hutchinson, and Ross, Inc., Stroudsburg (1973).

[71] W. Yang, and R. G. Parr, Hardness, softness, and the fukui function in the electronic theory of metals and Catalysis Proc. NatL Acad Sci USA., **82**, 6723, (1985).

[72] R.G. Parr, L.V. Szentpaly, and S. B. Liu, Electrophilicity Index J. Am. Chem. Soc., **121**, 1922 (1999).

[73] (Chattaraj, P. K.; Sarkar, U, and D.R. Roy, Electrophilicity Index D. R. Chem. Rev.,**10**6, 2065, (2006).

[74] P.K. Chattaraj and D.R. Roy, Update 1 of Electrophilicity Index Chem. Rev., **107**, 46 (2007).